TABLE 1. Patients and Samples

Patient No.	Filament Location	Number of Filaments Collected	Age	Sex	Underlying Cause of Filament	Current Treatment at Time of Filament Removal	Photos
1	Upper	2	85	F	OCP	AT	Fig. 2
2	Upper	1	50	F	PKP	AT+OFLX+BETA	Figs. 1A, 1B, 3A-C3, 4A-D3, 5A-G1, 6A-C1
3	Upper	2	84	F	OCP	AT+OFLX+FLM+BETA+PSL	Figs. 1C, 1D, 3A-C4, 4A-D4, 5A-G2, 6A-C2
4	Lower	1	60	F	ATD	AT+LVFX+FLM	Figs. 1E, 1F, 3A-C5, 4A-D5
5	Lower	1	54	F	ATD	AT+LVFX+FLM+HYA	Figs. 3D-J, 4E, 4F
6	Lower	2	88	M	ATD	AT+LVFX+FLM	Figs. 5A-G3, 6A-C3
7	Upper	2	77	M	PKP	LVFX+FLM	
8	Upper	1	51	M	VS	LVFX+BETA+OFLXO	
9	Lower	1	78	F	ATD	AT+LVFX+FLM	
10	Lower	1	69	F	ATD	AT+LVFX+FLM	
11	Lower	1	71	F	ATD	AT+LVFX+FLM	
12	Lower	1	58	F	ATD	AT+OFLX+FLM	
13	Lower	1	49	F	ATD	AT+LVFX+FLM	

Upper, behind upper eye lid; Lower, behind lower eye lid; OCP, ocular cicatricial pemphigoid; ATD, aqueous tear deficiency; VS, vitreous surgery; AT, artificial tear; OFLX, 0.3% ofloxacin eye drop; BETA, 0.1% betamethasone sodium phosphate eye drop; FLM, 0.02% fluorometholone eye drop; PSL, prednisolone tablets; LVFX, 0.5% levofloxacin eye drop; HYA, 0.3% sodium hyaluronate eye drop; OFLXO, 0.3% ofloxacin eye ointment.

IgG1, IgG2a, IgG2b (DakoCytomation, Kyoto, Japan), and goat IgG (Santa Cruz Biotechnology Inc., Santa Cruz, CA) as negative controls. After a 1-hour incubation, the sections were washed with 0.01 M PBS and then treated with fluorescent secondary antibody solutions (Alexa-488- or 594-labeled anti-mouse IgG or anti-goat IgG; Invitrogen, Carlsbad, CA). After a 1-hour incubation, the sections were washed with 0.01 M PBS, and the nuclei were stained with propidium iodide or DAPI and mounted with medium containing 3% anti-photo-bleaching reagent (DABCO; Wako Pure Chemical Industries, Ltd., Osaka, Japan). Unless otherwise stated, all incubations were performed at room temperature. Some filaments were embedded in paraffin wax by standard procedures. The paraffin-embedded sections (4 μm) were stained with HE. Fluorescent and HE-stained images of the sections were taken by microscope with a cooled CCD camera (Olympus Corp., Tokyo, Japan). A commercial fluorometric TUNEL system (DeadEnd; Promega, Madison, WI) was used for analysis of apoptosis.

RESULTS

Slit Lamp Examination

Slit lamp examination of the 13 patients with filamentary keratitis revealed filaments of various sizes. Almost all the big filaments found on the patients' corneas were located behind the upper or lower eye lids (Fig. 1E, Table 1). Whole images of these filaments were observable when fingers were used to open patients' lids (Figs. 1A–D, 1F).

TABLE 2. Antibodies

Group	Antigen	Final Concentration μg/mL	Type of Antibody	Immunized Animal	Company	Annotation
Cytokeratins	CK1	0.025	Mo	M	Novocastra	Major cytokeratin in skin epidermis
	CK4	4.5	Mo	M	Novocastra	Major cytokeratin in nonkeratinizing mucosal epithelium
	CK6	1.0	Mo	M	Novocastra	Expressed at wound healing or hyperproliferative situation
	CK10	0.30	Mo	M	Novocastra	Major cytokeratin in skin epidermis
	CK12	2.0	Po	G	Santa Cruz	Major cytokeratin in cornea
	CK13	2.3	Mo	M	Novocastra	Major cytokeratin in nonkeratinizing mucosal epithelium
Mucin	MUC1	3.4	Mo	M	ZYMED	A membrane-bound mucin
	MUC4	1.0	Mo	M	ZYMED	A membrane-bound mucin
	MUC5AC	0.55	Mo	M	Novocastra	Secreted mucin/goblet cell mucin
	MUC16	0.85	Mo	M	Abcam	A membrane-bound mucin
Infiltration cells	HLA-DR	1.7	Mo	M	Dako Cytomation	Marker of macrophage, Langerhans cell
	Neutrophil elastase	0.70	Mo	M	Dako Cytomation	Marker of neutrophil
Proliferation	Ki67	0.93	Mo	M	Dako Cytomation	Cell proliferation marker
Keratinization-related proteins	Transglutaminase-1	5.0	Mo	M	Blogenesis	Enzyme that catalyzes the cross-linking of envelope component proteins
	Filaggrin	0.25	Mo	M	Blogenesis	Serves as matrix for keratin 1/10 aggregation

Mo, monoclonal; Po, polyclonal; M, mouse; G, goat; Novacastra: Novocastra Laboratories, Ltd., Benton Lane, UK; ZYMED: Zymed Laboratories, Inc., South San Francisco, CA; Abcam: Abcam Co. Ltd., Tokyo, Japan; Biogenesis: Biogenesis Ltd., Poole, UK.

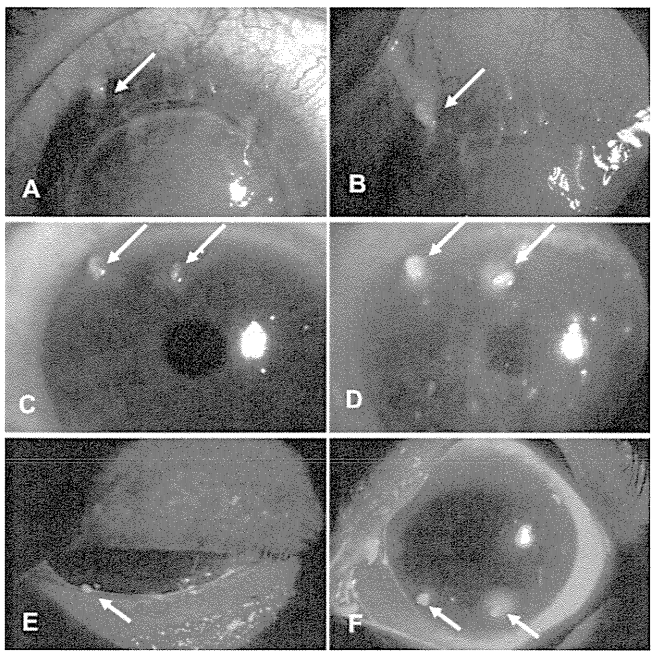

FIGURE 1. Slit lamp examination of filamentary keratitis. The photos are of representative cases of filamentary keratitis. (**A**, **B**) Post-PKP (case 2); (**C**, **D**) ocular cicatricial pemphigoid (case 3) and (**E**, **F**) ATD plus blepharoptosis (case 4). *Arrows*: large filaments.

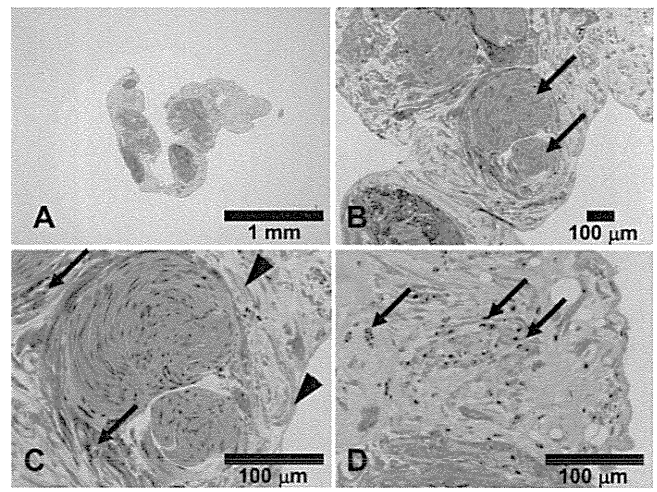

FIGURE 2. Paraffin-embedded HE staining of a filament. A filament taken from the patient with optical cicatricial pemphigoid + blepharoptosis (case 1) was fixed with 10% neutral buffered formalin, embedded in paraffin, sectioned, and stained with HE (hematoxylin eosin) (**A**–**D**). The filament consisted of a core composed of eosinophilic cells that have spindle-shaped cellular cytoplasm and nuclei (*arrows*; **B**). (**C**) The surrounding parts were basophilic fibers (*arrows*) and faint basophilic acellular areas that included basophilic segments (*arrowheads*); (**D**) many cells had polymorphic nuclei (*arrows*).

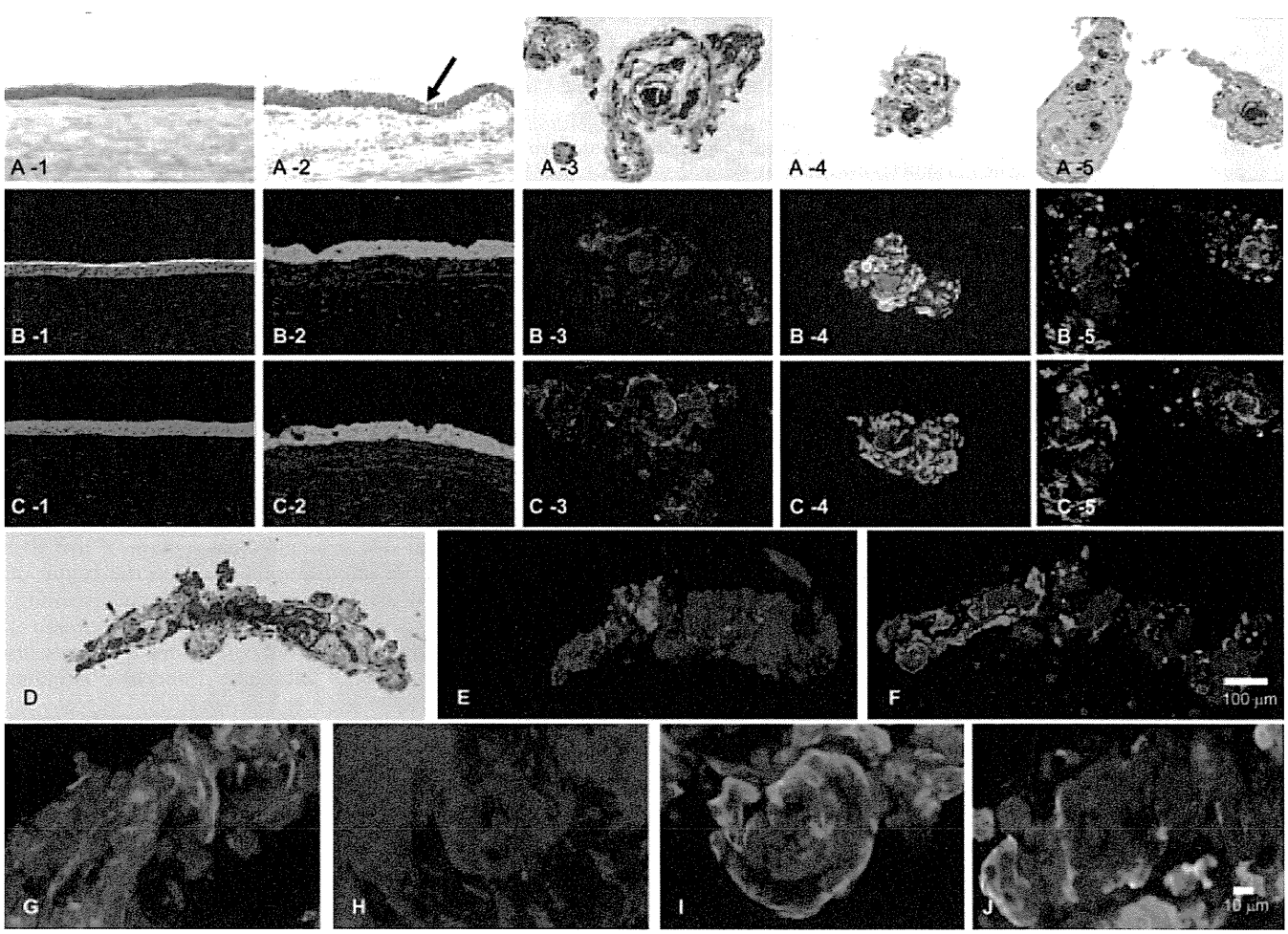

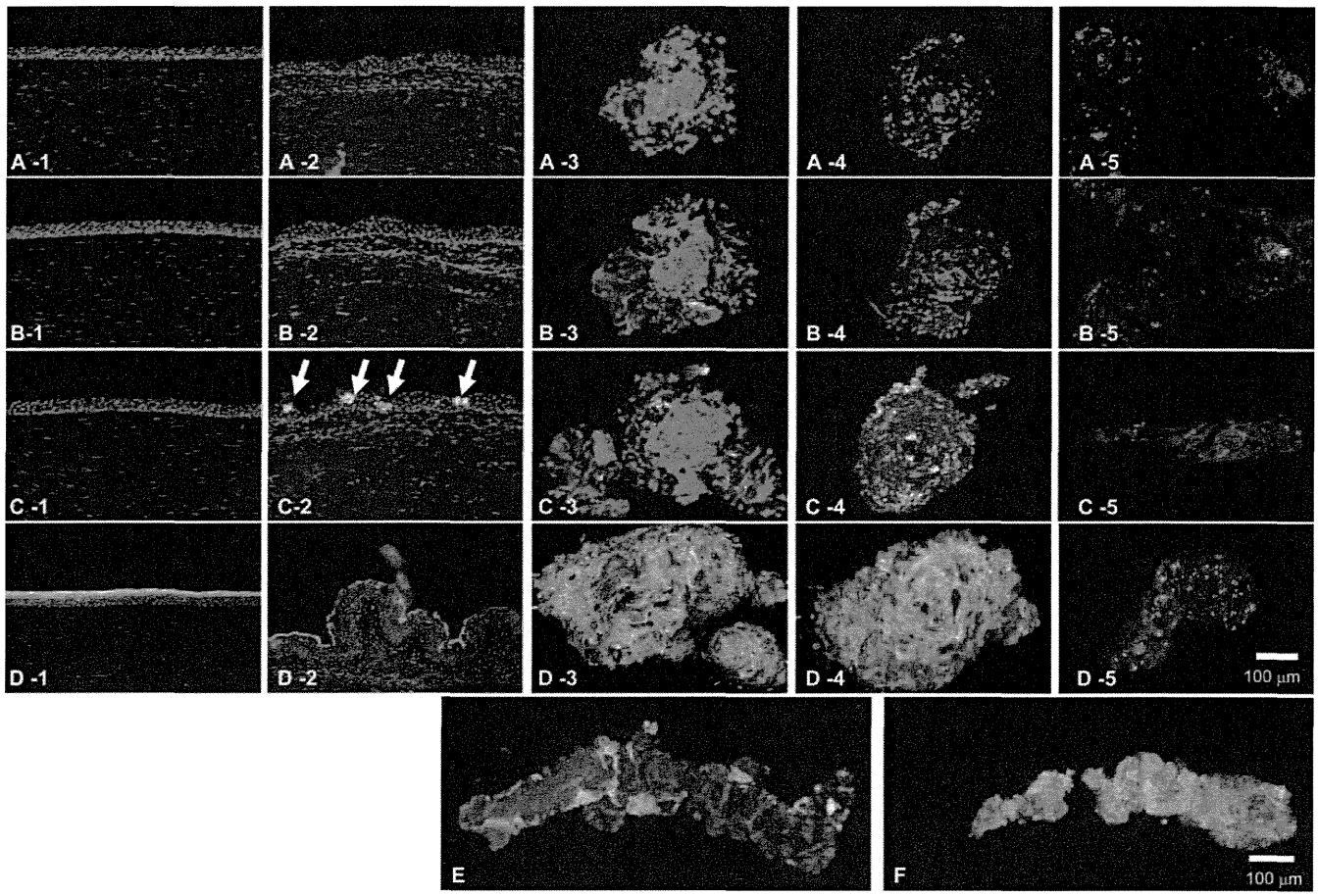

FIGURE 4. The distribution of mucins. (**A**) MUC1/nuclei (*green/red*); (**B**) MUC4/nuclei (*green/red*); (**C, E**) MUC5AC/nuclei (*green/red*); (**D, F**) MUC16/nuclei (*green/red*). (**1**) Corneal epithelium and (**2**) conjunctival epithelium. Filaments in (**3**) a post-PKP eye (case 2), (**4**) an ocular cicatricial pemphigoid eye (case 3), and (**5**) an ATD eye (case 4). Staining for MUC1 and -4 was slightly positive on conjunctival epithelium (**A2, B2**); for MUC5AC was positive on conjunctival epithelium (**C2**) at the goblet cells and the area around the filaments (**C3-5, E**); and for MUC16 was positive on both corneal (**D1**) and conjunctival (**D2**) epithelia and almost all areas of the filaments (**D3-5, F**).

Light Microscopic Analysis

HE staining of paraffin-embedded sections showed that the filament consisted of a core composed of eosinophilic cells that had spindle-shaped cellular cytoplasm and nuclei. The surrounding parts were basophilic fibers and faint basophilic acellular areas that included basophilic segments and polymorphic nucleic cells (Fig. 2). The light microscopic images of HE-stained cryosections of each filament and of normal cornea and conjunctiva showed similar patterns to the patterns shown in the immunostaining images (Figs. 3A1–5). The histologic images of the cryosections were similar to those of the paraffin-embedded sections. The filaments had eosinophilic cores, acellular areas, and basophilic segments. The normal cornea and conjunctiva had eosinophilic epithelium, and a pale goblet cell (Fig. 3A2, arrow) was found in the conjunctival epithelium.

Immunostaining

CK12 was expressed on all layers of normal corneal epithelium. CK4 was expressed on normal conjunctival epithelium and the superficial layer of normal corneal epithelium. Normal conjunctival epithelium was immunostained against CK13 (Fig. 3). In samples that had cores on HE-stained paraffin-embedded and frozen sections (Figs. 2, 3A3–5), the core areas strongly stained red, positive for CK12. In the areas surrounding the filaments, the cellular components strongly stained green, positive for CK4 and -13. A longitudinal section of the filament showed a long core of eosinophilic cells at the center of the filament under HE staining (Fig. 3D). By immunostaining, the red-stained CK12-positive corneal epithelium was found at the center of the filament. These red cores were of an inosculated, ropy, braided shape. The CK4- and -13-positive conjunctival

FIGURE 3. The distribution of the marker of corneal and conjunctival epithelium. (**A, D**) HE staining of the frozen sections (*arrow* indicates a goblet cell); (**B, E, G, H**) CK12/CK4/nuclei (*red/green/blue*); (**C, F, I, J**) CK12/CK13/nuclei (*red/green/blue*); (**A–C**) transverse sections; (**D–J**) longitudinal sections of filament; (**G, H**) magnified view of (**E**); and (**I, H**) magnified view of (**F**). (**1**) Corneal epithelium and (**2**) conjunctival epithelium. Filaments in (**3**) a post-PKP eye (case 2), (**4**) an ocular cicatricial pemphigoid eye (case 3), and (**5**) an ATD eye (case 4). Staining was positive for CK12 on the corneal epithelium (**B1**) and core area of the filaments (**B3-5, C3-5, E, F**); for CK4 on the conjunctival epithelium (**B2**), the superficial epithelium of the cornea (**B1**), and the area around the filaments (**B3-5**); and for CK13 on the conjunctival epithelium (**C2**) and the area around the filaments (**C3-5**). These red cores were of an inosculated, ropy, braided shape (**G, J**). *Blue*: nuclear and DNA fibers.

epithelium, which were stained green, were found in the area around the corneal cells. The side of the attachment site had round or elliptical nuclei stained blue, but the side of the free extremity had a fiber form stained blue by DAPI (Figs. 3D–J). MUC1 and -4 were slightly positive in the conjunctival epithelium, MUC5AC was positive in conjunctival epithelium at the goblet cells, and MUC16 was positive in both the corneal and conjunctival epithelia (Figs. 4A–D1, A–D2). We detected a considerable amount of MUC5AC (goblet-cell–derived, gel-forming mucin) in the acellular area of the filaments, MUC16 (membrane-bound mucin in the corneal and conjunctival epithelium) in almost all areas (Figs. 4C, 4D), but a limited amount of MUC1 and -4 in the filament itself (Figs. 4A, 4B). Moreover, MUC5AC and -16 stained positive in the longitudinal section, and the side of the free extremity had a fiber form that was stained red by PI (Figs. 4E, 4F). Infiltrating cells were positive for neutrophil elastase or HLA-DR. The surrounding areas stained weakly for CK6, which was expressed at wound healing or in a hyperproliferative situation; stained faintly for CK1 and -10, which are major cytokeratins in the epidermis of the skin; and stained not at all for keratinization-related protein (TGase-1 and filaggrin; Fig. 5). The nuclei of the core areas and PI-positive fibrous material around the core were TUNEL positive, but were negative without the rTdT enzyme. These nuclei did not stain for the cell proliferation marker Ki67 (Fig. 6).

Negative control experiments were used for immunostaining under the same conditions used for each antibody, and they showed no positive staining.

A summary of the histological data is shown in Table 3.

Discussion

Wright[8] showed by PAS, Alcian blue, and red oil staining that most of the filaments of filamentary keratitis are composed of mucus with epithelial squamous, lipids, and foreign matter taken up secondarily. Lambert [13,14] reported a theory about the formation of filaments, and that theory has subsequently been included in various textbooks.[2,3] As a normal epithelial surface degenerates due to desiccation, some cells die and fall off, thus leaving a defect. Mucin may adhere to this high-energy pit, and eventually epithelium may grow over the mucin to form a filament. However, Thiel et al.[10] and Zaidman et al.[11] presented another theory pertaining to filamentary keratitis by transmission electron microscopy of a patient with a brain stem disease, which showed that groups of inflammatory cells and fibroblasts were present just below the basal epithelium. It appears that these cells had disrupted the epithelial basement membrane and Bowman's layer. These findings support the theory that filamentary keratitis is associated with the damage of basal epithelial cells, epithelial basement membrane, or both. These findings regarding the components of the filament were derived from classic staining and electron microscopic examination, although they were not enough to completely elucidate the detail and origins of the components. The mechanisms of filament generation that are different from our proposal may be due to these different methods and samples. Therefore, to further elucidate the components of the filament, we examined the filament with an immunostaining technique.

HE staining of the paraffin-embedded sections clearly showed the filament to consist of a core composed of cells that had spindle-shaped, eosinophilic cytoplasm and nuclei. The surrounding parts were basophilic fibers and faint basophilic acellular areas that included basophilic segments and inflammatory cells. Our study revealed that the filament core was composed of corneal epithelium, a finding supported by positive staining for CK12, which is specifically expressed in corneal epithelium. On the other hand, the surrounding portion of the filament was composed mainly of degenerating conjunctival epithelial cells, which had markers typical of conjunctival epithelial cells[15] and did not have markers typical of corneal epithelium. It is also reasonable to speculate that the conjunctival epithelial cells surrounding the filament were mainly derived from the bulbar conjunctival epithelium that is next to the peripheral corneal epithelium and the palpebral

Table 3. Results of Histological Examination

Stain/Antigen	Number	Filament*						
HE (Paraffin Section)	1	Core Eosinophilic Spindle-Shaped Cells	Basophilic Fibers	Faint Basophilic Acellular Areas	Basophilic Segment	Polymorphic Nuclei Cells		
HE (Cryosection)	12	Eosinophilic	Basophilic Fibers	Faint Basophilic	Basophilic	Eosinophilic/ Basophilic	Corneal Epithelium	Conjunctival Epithelium
CK12	12	12	–	–	–	–	++	–
CK4	12	–	–	–	12	–	+ (S)	++
CK13	12	–	–	–	12	–	–	++
Muc1	4	–	–	–	4	–	–	+
Muc4	11	–	–	–	11	–	–	+/–
Muc5AC	12	–	–	12	12	–	–	++ (goblet)
Muc16	12	12	–	12	12	–	++ (S)	++ (S)
Neutrophil elastase	11	–	–	–	–	11		
HLA-DR	4	–	–	–	–	4		
CK1	4	4	–	–	–	–		
CK6	4	4	–	–	4	–		
CK10	4	–	–	–	4	–		
Filaggrin	3	–	–	–	–	–		
Transglutaminase-1	3	–	–	–	–	–		
TUNEL	3	3	3	–	3	3		
Ki67	3	–	–	–	–	–		

* Data shown in the Filament are the number that is positive. –, negative; +/–, slightly positive; +, moderately positive; ++, strongly positive; S, superficial.

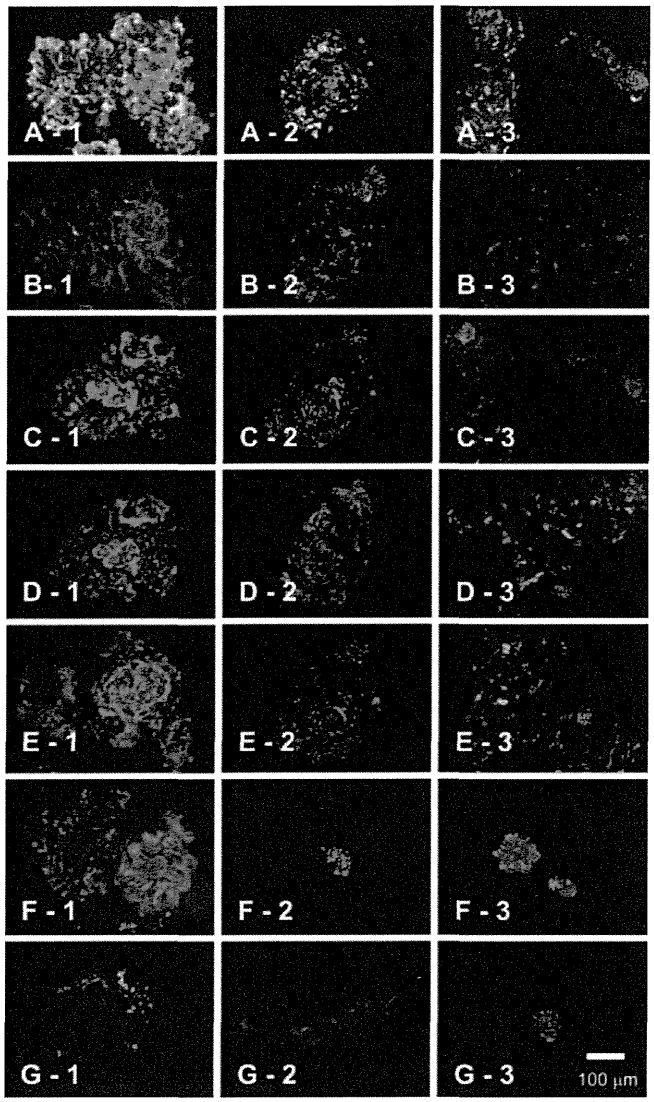

FIGURE 5. Immunostaining of the marker of inflammation cells, keratins, and keratinization-related protein. (**A**) Neutrophil elastase; (**B**) HLA-DR; (**C**) CK1; (**D**) CK6; (**E**) CK10; (**F**) filaggrin; and (**G**) TGase-1. Filaments in (**1**) a post-PKP eye (case 2), (**2**) an optical cicatricial pemphigoid eye (case 3), and (**3**) an ATD eye all stained *green* and the nuclei stained *red* (case 6). The surrounding areas stained for neutrophil-elastase (**A**) and HLA-DR (**B**), stained weakly for CK6 (**D**), stained faintly for CK1 (**C**) and CK10 (**E**), and did not stain at all for keratinization-related protein (**F**, **G**).

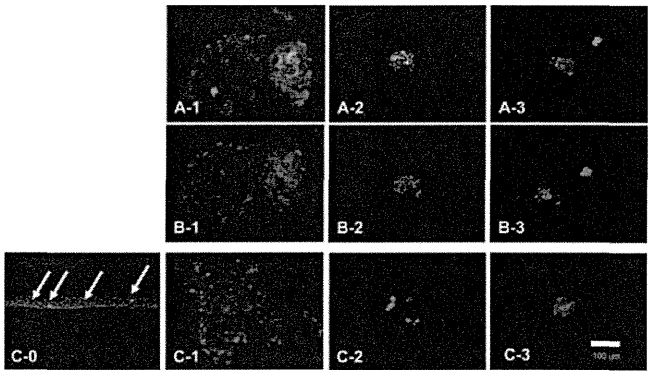

FIGURE 6. TUNEL staining and immunostaining with Ki67. (**A1–3**) TUNEL staining: The nuclei of the core areas and PI-positive fibrous material around the core stained positively for TUNEL, but (**B1–3**) stained negatively without the rTdT enzyme. (**C0**) Some human corneal epithelial cells stained for Ki67 (*arrows*). Filaments of (**C1**) a post-PKP eye (case 2), (**C2**) an optical cicatricial pemphigoid eye (case 3), and (**C3**) an ATD eye (case 6) did not stain clearly for Ki67.

conjunctival epithelium that is always in contact with the corneal surface. At the interface between the tear film and ocular surface epithelium, it was demonstrated that membrane-associated mucins, including MUC1, -4, and -16, and a major mucin of the secretory class, the goblet-cell–derived gel-forming MUC5AC, were all present,[16–20] and our study demonstrated that MUC5AC and -16 were the major mucins in the filament. MUC16 is expressed in the superficial corneal epithelium and conjunctival epithelium, and it was found in every part of the filaments in our study. CK1 and -10, although typical of epidermal keratinocytes, have also been described in corneal differentiated cells.[21] Previously, we have shown that the conjunctival epithelium in Sjögren's syndrome expresses the keratinization marker or keratinization-related proteins CK1, CK10, TGase-1, and filaggrin.[22] However, in this study we found that those proteins were expressed in the filaments in only a limited amount.

It is also known that filamentary keratitis is often associated with ocular surface inflammation. Our study reaffirmed that association and also demonstrated the existence of neutrophil and HLA-DR-positive cells in the filament. The structural rigidity of the filament, which is assumed to be the result of the twisted form of its core that is additionally supported by the surrounding mucin and the fiber of DNA from postlesional nuclei, is resistant to the condition of repeated friction by the eyelid. Moreover, although it has not been noted in previous reports, the DNA fiber, which exists mainly in the free extremity of the filament and is mixed with mucin, may be essential for the generation of the filament.

Since the large filaments that we were able to collect for this experiment were located behind the upper or lower eye lids, and the core from the corneal epithelium was seen to be of an inosculated, ropy, braided shape, it was thought that the filaments were formed by some mechanical energy. On the ocular surface, we speculate that the mechanical energy was the blinking of the eyelids and/or movement of the eye behind the eyelids.

In summary, although our new theory about the mechanism behind filament generation diverges from that previously reported,[11,13,14] our immunohistologic study of a large number of filament samples obtained from the cornea have led us to the

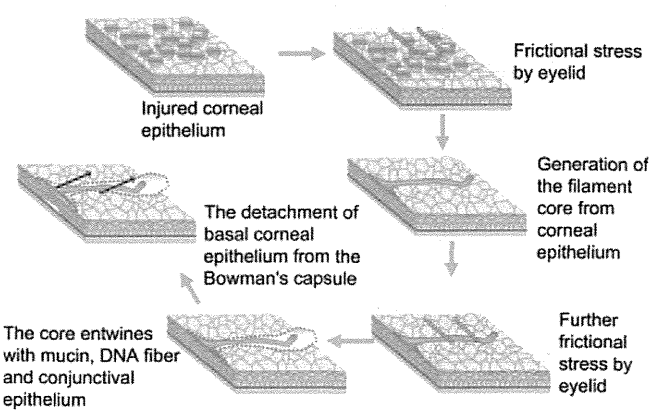

FIGURE 7. Schema for proposed mechanism of filament generation.

following conclusion. We hypothesize that filament generation starts from an injury to the surface epithelium of the cornea due to various disease conditions. Subsequently, friction cause by blinking and/or movement of the eye develops between the palpebral conjunctiva and the injured epithelium and produces the filament core. Further frictional stress is exerted by the eyelid, and the core then entwines with mucin, conjunctival epithelium, fiber of DNA from postlesional nuclei, and inflammatory cells, thus building up the filament. This phenomenon is sometimes associated with inflammation and the detachment of basal cells from the Bowman's layer due to blink- or eye-movement-related mechanical friction (Fig. 7). We believe that the results of this research will open new pathways toward understanding the mechanism that generates the filament in filamentary keratitis, as well as new methods of treatment in the future.

Acknowledgments

The authors thank John Bush for reviewing the article and the Northwest Lion's Eye Bank foundation for helping to obtain fresh human corneal tissues.

References

1. Beetham WP. Filamentary keratitis. *Trans Am Ophthalmol Soc.* 1935;33:413-435.
2. Kinoshita S, Yokoi N. Filamentary keratitis. In: Foster CS, Azar DT, Dohlman CH, eds. *Smolin and Thoft's the Cornea: Scientific Foundations and Clinical Practice.* 4th ed. Philadelphia: Lippincott Williams & Wilkins; 2005.
3. Davidson RS, Mannis MJ. Filamentary keratitis. In: Krachner JH, Mannis MJ, Holland EJ, eds. *Cornea.* 2nd ed. Philadelphia: Elsevier Mosby; 2005.
4. Albietz J, Sanfilippo P, Troutbeck R, Lenton LM. Management of filamentary keratitis associated with aqueous-deficient dry eye. *Optom Vis Sci.* 2003;80:420-430.
5. Diller R, Sant S. A case report and review of filamentary keratitis. *Optometry.* 2005;76:30-36.
6. Kakizaki H, Zako M, Mito H, Iwaki M. Filamentary keratitis improved by blepharoptosis surgery: two cases. *Acta Ophthalmol Scand.* 2003;81:669-671.
7. Maudgal PC, Missotten L, Van Deuren H. Study of filamentary keratitis by replica technique. *Albrecht Von Graefes Arch Klin Exp Ophthalmol.* 1979;211:11-21.
8. Wright P. Filamentary keratitis. *Trans Ophthalmol Soc U K.* 1975; 95:260-266.
9. Tanaka Y, Danjyo S, Hara J, Tanaka R, Minekawa Y. Histological and virological studies of filamentary keratitis following cataract extension [in Japanese]. *Fol Ophthalmol Jpn.* 1983;34:986-990.
10. Thiel HJ, Blumcke S, Kessler WD. Pathogenesis of keratopathia filamentosa (keratitis filiformis): light and electron microscopy study (in German). *Albrecht Von Graefes Arch Klin Exp Ophthalmol.* 1972;184:330-344.
11. Zaidman GW, Geeraets R, Paylor RR, Ferry AP. The histopathology of filamentary keratitis. *Arch Ophthalmol.* 1985;103:1178-1181.
12. Gong H, Hayashida H, Amemiya T. Electron microscopic features of filamentary keratitis [in Japanese]. *Jpn Rev Clin Ophthalmol.* 2000; 94:454-456.
13. Lamberts DW. Dry eye syndromes. In: Foster CS, ed. *Cornea and External Disease.* Chicago: Year Book Medical Publishers; 1985.
14. Lamberts DW. Dry eyes, keratoconjunctivitis sicca. In: Smolin G, Thoft RA, eds. *The Cornea.* 2nd ed. Boston: Little, Brown & Co.; 1987.
15. Wei ZG, Sun TT, Lavker RM. Rabbit conjunctival and corneal epithelial cells belong to two separate lineages. *Invest Ophthalmol Vis Sci.* 1996;37:523-533.
16. Inatomi T, Spurr-Michaud S, Tisdale AS, Gipson IK. Human corneal and conjunctival epithelia express MUC1 mucin. *Invest Ophthalmol Vis Sci.* 1995;36:1818-1827.
17. Inatomi T, Spurr-Michaud S, Tisdale AS, et al. Expression of secretory mucin genes by human conjunctival epithelia. *Invest Ophthalmol Vis Sci.* 1996;37:1684-1692.
18. Inatomi T, Tisdale AS, Zhan Q, Spurr-Michaud S, Gipson IK. Cloning of rat Muc5AC mucin gene: comparison of its structure and tissue distribution to that of human and mouse homologues. *Biochem Biophys Res Commun.* 1997;236:789-797.
19. Gipson IK. Distribution of mucins at the ocular surface. *Exp Eye Res.* 2004;78:379-388.
20. Gipson IK, Inatomi T. Cellular origin of mucins of the ocular surface tear film. *Adv Exp Med Biol.* 1998;438:221-227.
21. Pearton DJ, Ferraris C, Dhouailly D. Transdifferentiation of corneal epithelium: evidence for a linkage between the segregation of epidermal stem cells and the induction of hair follicles during embryogenesis. *Int J Dev Biol.* 2004;48:197-201.
22. Hirai N, Kawasaki S, Tanioka H, et al. Pathological keratinisation in the conjunctival epithelium of Sjögren's syndrome. *Exp Eye Res.* 2006;82:371-378.

Enhancement on Primate Corneal Endothelial Cell Survival In Vitro by a ROCK Inhibitor

Naoki Okumura,[1] *Morio Ueno,*[1,2] *Noriko Koizumi,*[3] *Yuji Sakamoto,*[4] *Kana Hirata,*[3] *Junji Hamuro,*[1] *and Shigeru Kinoshita*[1]

Purpose. The transplantation of cultivated corneal endothelial cells (CECs) has gained attention recently for the treatment of patients with corneal endothelial dysfunction. However, an efficient culturing technique for human (H)CECs has yet to be properly established. The present study was conducted to investigate the applicability of the Rho kinase (ROCK) inhibitor Y-27632 in promoting cultivation of cynomolgus monkey (M)CECs.

Methods. MCECs of cynomolgus monkeys were cultured in a medium containing 10 μM Y-27632. The number of viable cells adherent to culture plates were monitored by a luminescent cell-viability assay and colony growth was detected by toluidine blue staining. Proliferating cells were detected by Ki67 expression using flow cytometry and a BrdU-labeling assay for immunocytochemistry. Annexin V-positive apoptotic cells were analyzed by flow cytometry.

Results. The number of viable cultivated MCECs was enhanced by Y-27632 addition after 24 hours in culture. The colony area of the culture in the presence of Y-27632 was higher than in the absence of Y-27632 on day 10. In Y-27632-treated cultures, the number of Ki67-positive cells was significantly increased at 24 and 48 hours, and the number of proliferating BrdU-positive cells was increased at 48 hours. The number of Annexin V-positive apoptotic cells was decreased at 24 hours.

Conclusions. The inhibition of Rho/ROCK signaling by specific ROCK inhibitor Y-27632 promoted the adhesion of MCECs, inhibited apoptosis, and increased the number of proliferating cells. These results suggest that the ROCK inhibitor may serve as a new tool for cultivating HCECs for transplantation. (*Invest Ophthalmol Vis Sci.* 2009;50:3680-3687) DOI:10.1167/iovs.08-2634

The corneal endothelium is essential for the maintenance of corneal transparency. Since human corneal endothelial cells (HCECs) have poor in vivo proliferative potency, corneal endothelial disorders such as Fuchs' endothelial dystrophy, pseudophakic bullous keratopathy, and trauma lead to a compensatory enlargement of the remaining endothelial cells and irreversible corneal endothelial dysfunction. Penetrating keratoplasty has been widely performed for the improvement of endothelial dysfunction; however, the procedure has several adverse effects such as the potential for irregular astigmatism, suture-induced problems, fragility against trauma, and invasiveness. Alternative methods for replacing the corneal endothelium have been developed, including posterior lamellar keratoplasty, deep lamellar endothelial keratoplasty, and Descemet's-stripping endothelial keratoplasty.[1-3] Although these methods provide considerable benefits clinically, allograft rejection and primary graft failure remain a problem. Moreover, the worldwide shortage of donors is critical. Recently, the transplantation of cultivated CECs has been suggested as an alternative approach to the treatment of corneal endothelial dysfunction. The transplantation of cultured HCECs as a sheet, with[4,5] or without[6] a carrier, and the injection of progenitor cells[7,8] has been explored in animal studies. However, the animal model used in these studies was the rabbit, in which CECs retain high-proliferation ability, and in which residual peripheral CECs proliferate rapidly after injury and regenerate a clear cornea.[9] Aiming to establish a nonhuman primate model with poorly proliferative CECs, we recently reported a cynomolgus monkey model of cultivated CEC sheet transplantation.[10]

However, efficient culture techniques of HCECs need further development before practical application. HCECs are arrested at the G_1-phase of the cell cycle,[11,12] and an age-dependent negative regulation of the cell cycle might causally contribute to the poor proliferative activity in vitro.[13-15] Several studies have reported the successful cultivation of HCECs by use of an animal-derived extracellular matrix (ECM).[16-18]

To establish a clinically applicable efficient way to cultivate HCECs free of animal-origin pathogens, we focused our study on modulating the activity of GTPase Rho, regulating cell-to-substrate and cell-to-cell adhesions.[19-21] Rho and Rho-associated kinases (ROCKs) have a critical function in regulating cell adhesion and cell motility.[22,23] ROCKs are essential in regulating focal adhesions in cultured fibroblasts and epithelial cells.[24] The Rho subfamily contributes to the regulation of many different biological processes through actin-myosin-mediated contractile force generation via the phosphorylation of downstream target proteins.

In terms of other biological effects, Rho GTPases are well known to play a crucial role in cell-cycle progression and in apoptosis. It was initially reported that Rho inactivation blocks G_1-S phase progression and that the microinjection of active RhoA into quiescent cells induces G_1-S phase progression in Swiss 3T3 fibroblasts.[25] Although the underlying mechanism has yet to be thoroughly revealed, ROCK signaling is thought to promote cell-cycle progression in various cell types,[25,26] including CECs.[27] Unlike these reported findings, we have found that inhibition of the ROCK pathway by a selective

From the [1]Department of Ophthalmology, Kyoto Prefectural University of Medicine, Kyoto, Japan; the [2]Department of Ophthalmology, National Center for Geriatrics and Gerontology, Obu, Japan; the [3]Department of Biomedical Engineering Faculty of Life and Medical Sciences, Doshisha University, Kyotanabe, Japan; and the [4]Research Laboratory, Senju Pharmaceutical Co., Ltd., Kobe, Japan.

Supported in part by the Academic Frontier Research Project on the New Frontier of Biomedical Engineering Research and by Grant-in-Aid for Scientific Research 16791076 from the Japanese Ministry of Education, Culture, Sports, Science, and Technology.

Submitted for publication July 29, 2008; revised November 18, 2008, and February 25, 2009; accepted June 22, 2009.

Disclosure: **N. Okumura**, None; **M. Ueno**, None; **N. Koizumi**, None; **Y. Sakamoto**, None; **K. Hirata**, None; **J. Hamuro**, None; **S. Kinoshita**, None

The publication costs of this article were defrayed in part by page charge payment. This article must therefore be marked "*advertisement*" in accordance with 18 U.S.C. §1734 solely to indicate this fact.

Corresponding author: Morio Ueno, Department of Ophthalmology, Kyoto Prefectural University of Medicine, Kyoto 602-0841, Japan; mueno@koto.kpu-m.ac.jp.

Investigative Ophthalmology & Visual Science, August 2009, Vol. 50, No. 8

inhibitor of ROCK, Y-27632, promotes proliferation as well as adhesion of MCECs and inhibits apoptosis.

Materials and Methods

Animal Experiment Approval

In all experiments, animals were housed and treated in accordance with the ARVO Statement for the Use of Animals in Ophthalmic and Vision Research. The experimental procedures were approved by the committee for Animal Research at Kyoto Prefectural University of Medicine.

Primary Cultures

We used eight corneas from four cynomolgus monkeys (3–5 years of age; estimated equivalent human age, 5–20 years) housed at Nissei Bilis Co., Ltd. (Otsu, Japan) and Keari Co., Ltd. (Wakayama, Japan). The corneas were harvested at the time of euthanatization of the monkeys for other research purposes, and the cells were placed in culture within 12 hours. We cultivated MCECs according to a modified protocol of HCEC culture reported previously.[5] Descemet's membrane was stripped of intact MCECs and transferred to 0.6 U/mL of Dispase II (Roche Applied Science, Penzberg, Germany). After a 60-minute incubation at 37°C, the MCECs obtained from individual corneas were resuspended in culture medium and were plated in 1 well of a 12-well plate. All primary cell cultures and serial passages of MCECs were performed in growth medium composed of Dulbecco's modified Eagle's medium (DMEM) supplemented with 10% fetal bovine serum (FBS), 50 U/mL penicillin, 50 μg/mL streptomycin, and 2 ng/mL basic fibroblast growth factor (bFGF; Invitrogen Corp., Carlsbad, CA). MCECs were cultured in a humidified atmosphere at 37°C in 5% CO_2. The culture medium was changed every 2 days. When cells reached confluence in 10 to 14 days, they were rinsed in Ca^{2+} and Mg^{2+}-free Dulbecco's phosphate-buffered saline (PBS), trypsinized with 0.05% trypsin-EDTA (Invitrogen) for 5 minutes at 37°C, and passaged at ratios of 1:2 to 4.

Determination of the Number of Viable Cells

The number of viable cells was determined by a cell-viability assay (CellTiter-Glo Luminescent Cell Viability Assay; Promega Corp., Madison, WI) using the recommended protocol. Viability assays that generate luminescent signals are based on quantification of the ATP levels. MCECs were plated at a density of 2.0×10^3 cells onto 96-well plates. An equal volume of the chemiluminescent reagent was added to 100 μL of medium containing cells for each 96-well plate. Luminescence in each well was measured by a luminometer (Veritas Microplate Luminometer; Turner Biosystems, Sunnyvale, CA) and was standardized to the luminescence of the control. Analyses were performed on the first day of passage and five samples were prepared for each group.

Colony-Forming Efficiency

The clonal growth ability of primary MCECs was determined by the colony-forming efficiency (CFE). Cells were plated at a density of 2.0×10^3 cells/cm^2. Then, the colonies were fixed on day 11 and stained with 0.1% toluidine blue, and the accumulated area was analyzed by Image J software (developed by Wayne Rasband, National Institutes of Health, Bethesda, MD; available at http://rsb.info.nih.gov/ij/index.html). CFEs were expressed as the multiple of change between the control and treated areas. Five samples were prepared for each group.

Immunohistochemistry

Cultured MCECs on chamber slides (Laboratory-Tek; NUNC A/S, Roskilde, Denmark) were fixed in 4% formaldehyde for 10 minutes at room temperature (RT), permeabilized for 5 minutes in PBS containing 0.1% Triton X-100, washed, and incubated for 30 minutes with 1% bovine serum albumin (BSA). For actin studies, the MCECs were incubated at 4°C overnight with a 1:400-dilution rhodamine-conjugated phalloidin molecular probe (Invitrogen) and again washed three times with PBS. For Ki67 and actin double-staining studies, after blocking, the MCECs were incubated at RT with 1:400-dilution rhodamine-conjugated phalloidin (Invitrogen), washed with PBS three times, incubated overnight at 4°C with 1:400-dilution anti-mouse Ki67, and washed again three times. They were then incubated at RT with 1:2000-diluted Alexa Fluor 488-conjugated goat anti-mouse IgG (Invitrogen) and washed three times. During all steps, the endothelial side was face up to avoid damage. After they were washed with PBS in the dark, the specimens were mounted on glass slides with antifade mounting medium containing DAPI (Vector Laboratories, Burlingame, CA), and the slides were inspected with a fluorescence microscope (AX70; Olympus, Tokyo, Japan).

Flow Cytometry Analyses

For Ki67 studies, MCECs prepared as just described were passaged in 1:4 dilutions and cultured for 1 or 2 days. After this, the MCECs were dissociated to single cells by 0.25% trypsin digestion, fixed in 70% (wt/vol) ethanol, washed, and incubated for 20 minutes with 1% BSA. Then, the MCECs were incubated with 1:20-diluted anti-mouse Ki67, washed, and incubated with 1:1000-diluted Alexa Fluor 488-conjugated goat anti-mouse IgG (Invitrogen). For annexin V studies, MCECs were passaged in 1:4 dilutions, and all cells were dissociated to single cells by 0.25% trypsin digestion and recovered, including cells floating in the culture medium, at day 1. They were then subjected to an annexin V assay (Annexin V-FITC Apoptosis Detection Kit Plus; MBL Corp., Nagoya, Japan), according to the manufacturer's instructions. Flow cytometric analyses were then performed (FACSCalibur; BD Biosciences, Franklin Lakes, NJ).

BrdU-Labeling Assay

MCECs prepared as just described were passaged in 1:4 dilutions onto chamber slides (Laboratory-Tek; NUNC A/S), and cultured for 24 hours. They were then incubated for a further 24 hours with 1:1000-diluted 5-BrdU-labeling reagent (Amersham Biosciences, Buckinghamshire, UK). MCEC cultures were next washed in PBS, fixed for 30 minutes in acid-ethanol (90% ethanol; 5% acetic acid; 5% distilled water), washed

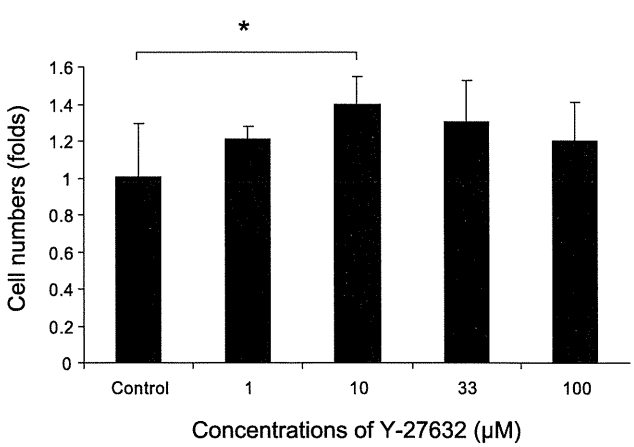

Figure 1. The enhanced survival of primary cultured MCECs by Y-27632. MCECs separated from Descemet's membrane were plated at a density of 2.0×10^3 cells/well in DMEM with 2 ng/mL bFGF. The number of viable MCECs attached to the plate at 24 hours was evaluated by luminescence assay of the ATP levels. Y-27632 at 10 μM resulted in significant cell-survival enhancement (*$P < 0.05$ vs. control). Data are expressed as the ratio to control cells and as the mean ± SE ($n = 5$).

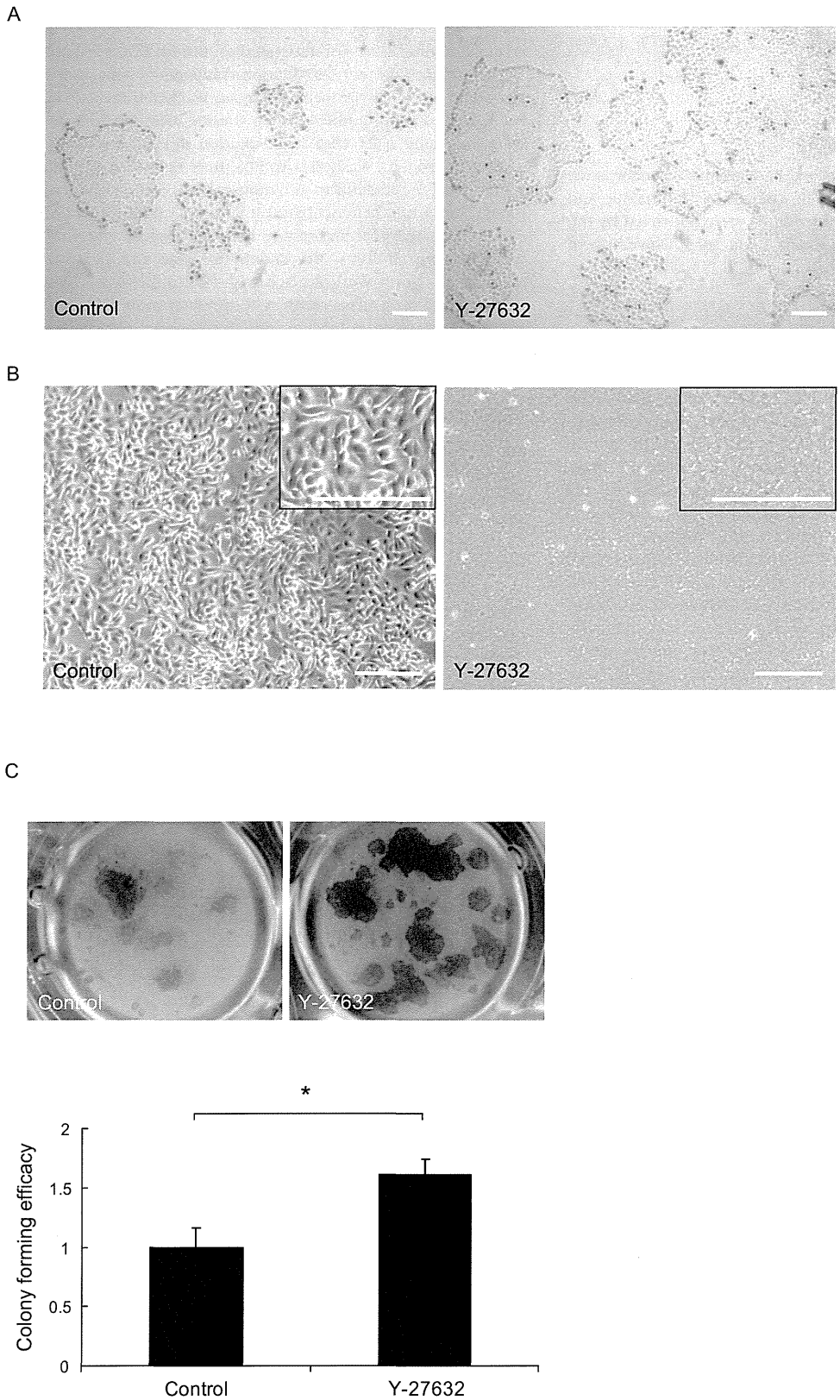

FIGURE 2. The improved culture efficacy of primary MCECs by Y-27632. (**A**, **B**) Primary MCECs from 4-year-old cynomolgus monkeys, prepared as shown in Figure 1, were plated at a density of 2.0×10^4 (**A**) or 2.0×10^5 (**B**) cells/well in the presence or absence of 10 μM Y-27632, and phase-contrast images were analyzed. *Insets*: higher magnification. Scale bar, 250 μm. (**C**) Colony growth of primary cultured MCECs. *Top*: the MCECs, prepared as above, were seeded at a density of 2.0×10^3 cells/cm^2 and stained with 0.1% toluidine blue on day 10. *Bottom*: colony areas of Y-27632–treated cells were elevated compared with those in control cultures (1.6-fold; $^*P < 0.01$). Data are expressed as the mean ± SE ($n = 5$).

with PBS, and incubated with 1% BSA at 37°C for 30 minutes to block nonspecific binding, followed by a 1-hour incubation at RT with mouse anti-BrdU antibody (Amersham Biosciences). After washing, they were then incubated, again at RT, with 1:2000-diluted Alexa Fluor 488–conjugated goat anti-mouse IgG (Invitrogen), washed three times, and mounted on glass slides with antifade mounting medium containing DAPI (Vector Laboratories). The slides were subsequently inspected with a fluorescence microscope.

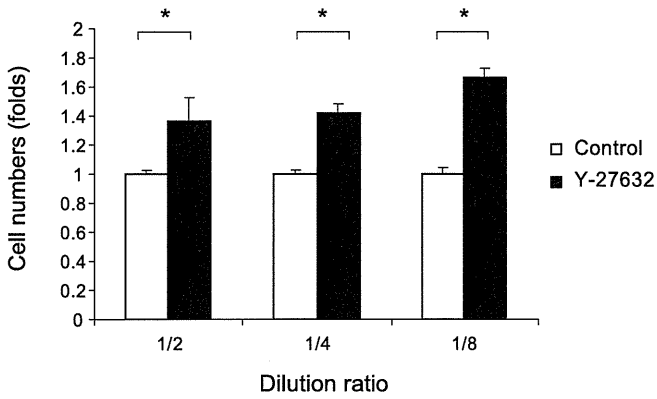

FIGURE 3. Y-27632 augmented the adherence of MCECs during subculture. MCECs, passaged four to six times, were diluted 1:2, 1:4, and 1:8 in the presence of 10 μM Y-27632. Viable cells attached 24 hours after the subculture were determined. The number of viable cells recovered was enhanced significantly in the presence of Y-27632 at all 3 dilutions ($^*P < 0.01$). Data are expressed as the mean ± SE ($n = 5$).

Statistical Analysis

The statistical significance (P) in mean values of the two-sample comparison was determined with Student's t-test. The statistical significance in the comparison of multiple sample sets was analyzed with the Dunnett multiple-comparisons test. Values shown on graphs represent the mean ± SE.

RESULTS

Primary Culture of MCECs

The numbers of viable primary MCECs attached on culture plates 24 hours after the start of the culture were monitored by a luminescent cell-viability assay. The number of viable primary MCECs adherent to the culture plate invariably increased over a wide range of concentrations, from 1 to 100 μM, of Y-27632. A commonly used working concentration of Y-27632,[28] 10 μM, resulted in the highest ($^*P < 0.05$ vs. control) cell-survival enhancement (Fig. 1).

Primary MCECs from 4-year-old cynomolgus monkeys prepared as described earlier were plated at a density of 2.0×10^4 cells/well in a 12-well plate in the presence or absence of 10 μM Y-27632, and phase-contrast images were analyzed. MCECs treated with Y-27632 showed better coverage on day 4 than did the nontreated groups (Fig. 2A). To further confirm the adhesion-improving effect, primary MCECs were seeded at a higher density (2.0×10^5 cells/well) in the presence or absence of 10 μM Y-27632. On day 3, untreated MCECs were proliferating and were enlarged, but were not confluent or homogeneously hexagonal. In contrast, Y-27632-treated MCECs exhibited a confluent monolayer of homogeneously hexagonal cells with smaller sizes (Fig. 2B). For an examination of the distinction of colony growth of primary MCECs between two culture groups with or without Y27632, MCECs were plated at a lower density of 2.0×10^3 cells/well in a 96-well microplate. On day 10, MCECs treated with Y-27632 demonstrated a markedly enhanced increase in colony growth, detected by toluidine blue staining (Fig. 2C). The colony area of Y-27632-treated cells was significantly higher than the control (1.6-fold, $^*P < 0.01$).

Subculture of MCECs

The number of viable primary MCECs adherent to the culture plate was invariably increased in the presence of Y-27632, indicating that there is a possibility that the application of Y-27632 may also improve the CFE of HCECs. To confirm the effect of Y-27632 during the culture passage, we next investigated the effect of Y-27632 on subcultured MCECs. Cultivated cells passaged 4 to 6 times in the presence of Y-27632 were diluted at three dilutions (1:2, 1:4, and 1:8), and the number of viable cells attached on the noncoated culture plate at 24 hours of subculture was then determined. It was found that the number of viable cells recovered was enhanced in the presence of Y-27632 at all three dilutions ($P < 0.01$; Fig. 3). It is of note that the enhancement ratio of adhesion to the plate tends to be higher at higher dilutions during passage. MCECs treated with Y-27632 during subculture showed enhanced cell adhesion both in phase-contrast images and in images of actin fibers immunostained with phalloidin antibody (Fig. 4).

The Effect of Y-27632 on Cell-Cycle Progression

Studies were conducted to determine whether Y-27632 might play a role in cell-cycle progression in MCECs. To answer this question, we first used immunostaining with the cell-cycle population marker Ki67. MCECs at confluence were passaged in 1:4 dilutions and subcultured for 1 or 2 days and were dissociated to single cells by trypsin digestion. MCECs subcultured in the culture medium with Y-27632 showed the presence of a larger number of Ki67-positive cells than was present in the controls (Fig. 5A). Actin immunostaining was also performed to determine whether there is a relationship between Ki67-positive cells and enhanced actin-fiber progression. It turned out that Ki67 expression had no direct relation to actin fibers. Further quantitative flow cytometric analysis revealed the increased presence of Ki67-positive cells in MCECs cultured with Y-27632, 2 days after subculture (Fig. 5B). A BrdU-labeling assay of 48-hour subcultures is shown in Figure 5C, and it shows a larger number of BrdU-positive MCECs among cell populations cultured with Y-27632 compared with control cells. Thus, it was demonstrated that Y-27632 plays a relevant role in the cell-cycle progression of MCECs.

The Effect of Y-27632 on Apoptosis

We next studied the involvement of Y-27632 in apoptosis. MCECs were passaged in 1:4 dilutions at the time of culture

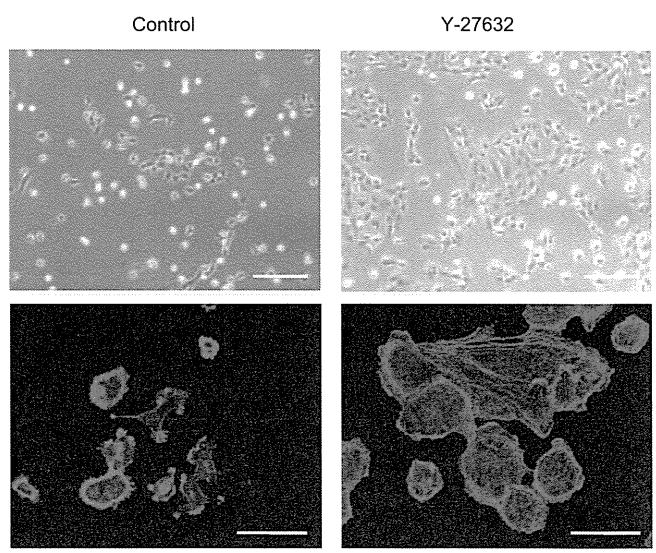

FIGURE 4. The morphologic change of passaged MCECs induced by Y-27632. *Top*: phase-contrast images of cells 24 hours after passage. *Bottom*: Immunostaining of actin in the same cells. Actin (*red*) and DAPI (*blue*). Scale bar: (**A**) 250 μm; (**B**) 50 μm.

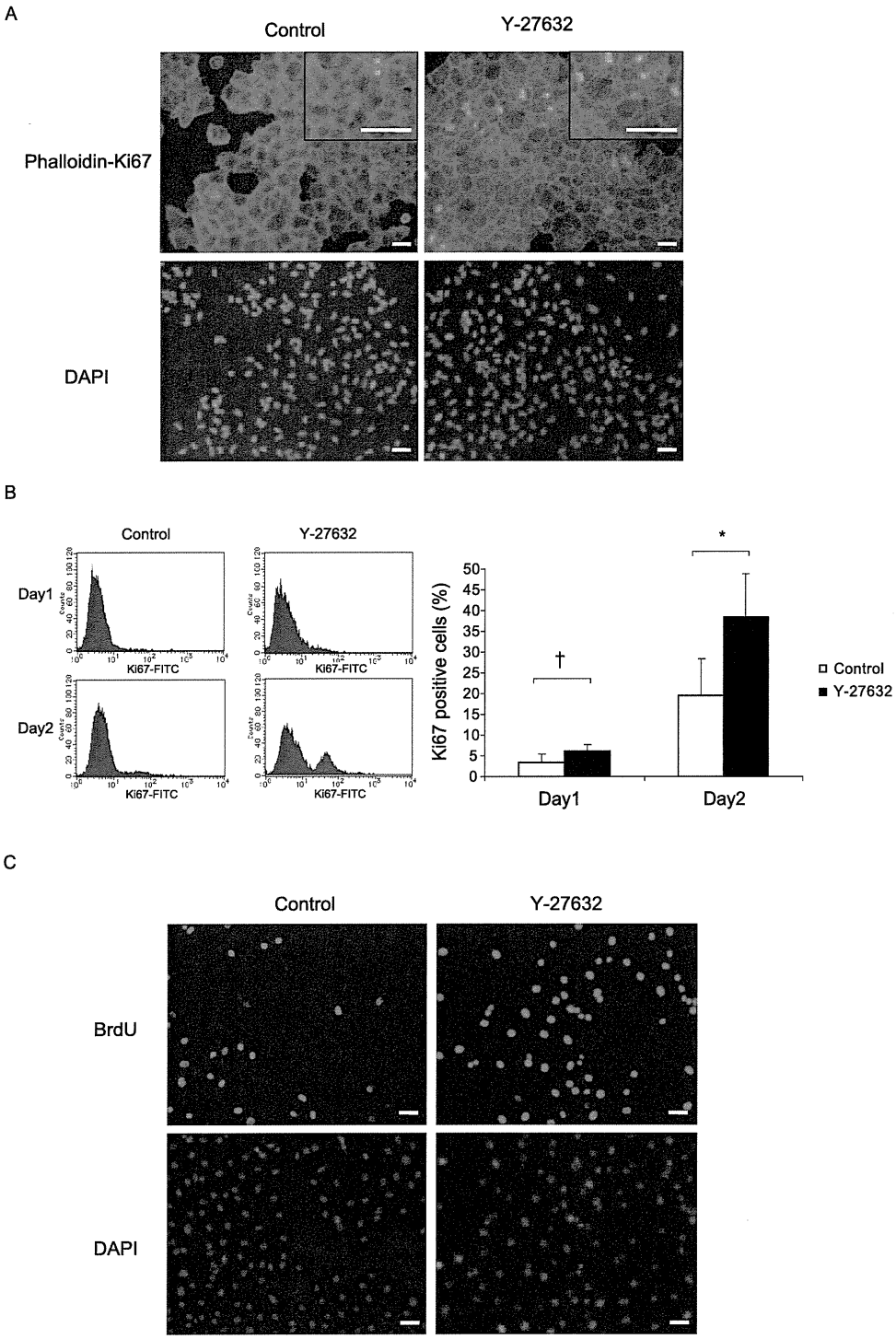

FIGURE 5. Increased frequency of proliferating MCECs by Y-27632. (**A**) Double immunostaining of Ki67 and actin fibers; the passaged MCECs were cultured for 48 hours and stained successively with Ki67 and phalloidin. Ki67 (*green*), actin (*red*), and DAPI (*blue*). *Inset*: higher magnification. (**B**) Ki67-positive cells were analyzed by flow cytometry. MCECs were subcultured for 1 or 2 days and stained successively with Ki67. The number of Ki67-positive cells was significantly elevated in the presence of Y-27632 on days 1 and 2 (†$P < 0.05$, *$P < 0.01$). Data are expressed as the mean ± SE ($n = 6$). (**C**) Y-27632 increased the frequency of BrdU-labeled MCECs. The MCECs were subcultured for 24 hours and incubated further for 24 hours with a 5-BrdU-labeling reagent, then stained with mouse anti-BrdU antibody. DAPI (*blue*). Scale bar: (**A**) 250 μm; (**C**) 100 μm.

confluence. All cells were then dissociated to single cells by trypsin digestion and recovered, including floating cells, 1 day after subculture in the presence of 10% FBS. The flow cytometry patterns of the annexin V assay revealed that Y-27632 treatment significantly decreased apoptosis ($P < 0.01$; Fig. 6A). The inhibition of apoptosis during culture without any stress load was lowered from 12.4% ± 4.6% in the control group to 2.0% ± 1.6% in the subculture group containing Y-27632, thus implicating the contribution of the apoptosis-reducing activity of Y-27632 to the efficient subculture of MCECs (Fig. 6B).

DISCUSSION

Inhibition of Rho/ROCK signaling by Y-27632 clearly promoted MCEC adhesion and inhibited apoptosis during culture. It also increased the proliferating cell population. These findings were confirmed with cynomolgus monkey-derived MCECs, which have poor proliferation potential, as do HCECs. MCECs are considered to be the preferable experimental tool for investigating nonproliferative HCECs, compared with rodent CECs or those derived from a rabbit

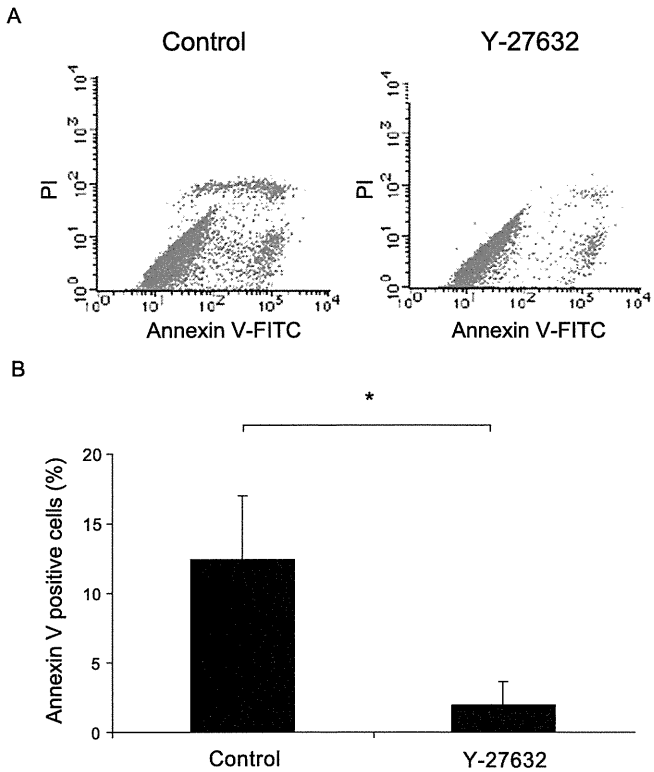

FIGURE 6. (**A**) Subcultured MCECs were dissociated to single cells by trypsin 24 hours after the subculture and subjected to annexin V assay. (**B**) The inhibition of apoptosis was lowered significantly from 12.4% ± 4.6% (control) to 2.0% ± 1.6% in the presence of Y-27632 (*$P < 0.01$). Data are expressed as the mean ± SE ($n = 4$).

in which the CECs retain a high proliferative ability both in vivo and in vitro.[7–9]

Although we found that MCECs tended to show a cell-senescence phenotype after only a few passages, we successfully cultivated and passaged MCECs in the presence of the ROCK inhibitor Y-27632. There have been several reports of successful CEC cultivation in which both explants[4,17] and cell suspensions[15] were used. There is almost no mitotic activity in the HCECs throughout the lifespan, and proliferation of adult HCECs cannot be achieved with standard cell-culturing techniques.[29] However, adult HCECs have been reported to proliferate when cultured with ECM derived from animals.[4,15,16] The fact that adult HCECs proliferate in the presence of ECM suggests that the interaction with the substratum is indispensable for the efficient growth and maintenance of MCECs.

In this context, it is of note that inhibition of the Rho/ROCK pathway by Y-27632 promotes cell adhesion to substrates of cultured THP-1 monocytes[19] and human Tenon fibroblast.[30] The actin cytoskeleton plays a critical role in cell adhesion,[19,30] which coincides well with our observation that the adhesion of cultured MCECs is promoted by Y-27632. We suspect that the enhanced adhesion by Y-27632 may be ascribable to the promotion of membrane protrusion by actin reconstitution[19,30] and to cell-to-cell adhesion by cadherin.[21] Further investigations on the underlying mechanism of the improved cell adhesion and the possible combined effect of Y-27632 with coated substrates such as ICAM-1, VCAM, collagen, fibronectin, and laminin[15,16,30] are likely to contribute much to further improvements in the efficacy of the culture of MCECs and HCECs.

Although the underlying mechanisms have yet to be thoroughly revealed, ROCK plays an important role in cell-cycle progression. ROCK activity is required for the formation of actin stress fibers that contribute to the sustained activation of Ras and the ERK mitogen-activated protein kinase (MAPK) after ligand stimulation.[31–33] In addition, RhoA promotes cell-cycle progression to S phase by regulating p27 degradation through its effect on cyclinE/CDK2 activity.[34] In HCECs, p27 is known to play a pivotal role in the negative regulation of cell-cycle progression.[11,12,35–37] However, and surprisingly, ROCK inhibition with Y-27632 promoted MCEC proliferation in our study (Fig. 5). Our finding that ROCK inhibition promotes the cell-cycle progression contrast with previously reported results.[25,31–33] This unexpected promotion of the cell-cycle progression of MCECs may be partially explained by the previous findings that the Rho/ROCK signaling, including cell proliferation, are cell-type-dependent.[38,39] It was illustrated that the blockade of sustained ERK/MAPK activity by inhibiting Rho and ROCK led to rapid cyclin-D1 induction through activation of Rac1 and Cdc42 in murine fibroblasts.[31,33] Although further studies are needed, cell adhesion and motility, which are enhanced by ROCK inhibition,[40] may have a positive effect on MCEC proliferation. Further investigations are necessary to determine whether the increased in cell proliferation observed in our studies can be ascribed to an effect on the molecular modules regulating cell-cycle progression.

ROCK is involved in the regulation of apoptosis.[38,41] Significant morphologic changes including contraction, membrane blebbing, and nuclear disintegration during apoptosis are driven by the ROCK-mediated actin-myosin contractile force.[42] ROCK inhibition has been reported to have an antiapoptotic effect in some models, such as a spinal cord injury model,[43] dissociated human embryonic stem cells,[44] and grafted neural precursors.[45] Recent research has highlighted the prosurvival effect of ROCK inhibitors for clinical use.[38] In this line, we confirmed the antiapoptotic effect of Y-27632 in cultivated MCECs. Reducing apoptotic cells during primary culture and passage procedures is beneficial, because a higher number of viable HCECs could be gained from a limited number of HCECs obtained from a donor in a clinical setting. However, ROCK inhibitors may induce apoptosis in specialized cell types,[46] including corneal epithelial cells.[47] Further research is needed to determine whether ROCK is a crucial target for these effects. The use of a ROCK $I^{-/-}$ and ROCK $II^{-/-}$ mouse model may clarify the contribution of kinase to apoptosis. HCECs with poor cell adhesion in the primary culture and in subcultures tend to show cell senescence with fibroblastic cell contamination.[16,18] Our preliminary observations indicate that MCECs assume the delayed cell-senescence phenotype during passage in the presence of Y-27632 (data not shown). Effective culture of HCECs from a limited number of donors is crucial for clinical use. Moreover, autologous CEC transplantation, obtained from a patient's fellow eye, will overcome allograft rejection. Our studies will be expanded to HCECs before clinical application, in combination with the previously reported CEC-sheet transplantation technique.[10] We predict that Y-27632 may be useful for the improved cultivation of HCECs. Of importance, no modification of the chromosome in Y-27632-treated cells has been reported,[44,48] and Y-27632, along with Fasudil, is already used clinically in cardiovascular therapies,[49] thus suggesting its safety in the clinical setting. Y-27632 is also reportedly effective in preventing fibroproliferation in glaucoma surgery[30] and as such may be an effective antiscarring agent after ocular surgery.

In summary, our results indicate that inhibition of Rho/ROCK signaling by the specific ROCK inhibitor Y-27632 promoted the adhesion of MCECs, inhibited apoptosis, and increased the frequency of proliferating cells. Our results with nonhuman primate CECs which have a low proliferative ability, similar to HCECs, raises the possibility that the ROCK inhibitor

may serve as a new tool in cultivating HCECs for newly emerging transplantation therapies.

Acknowledgments

The authors thank Yoshiki Sasai and Masatoshi Ohgushi for their assistance and invaluable advice about ROCK inhibitors and Hisako Hitora for technical assistance.

References

1. Melles GR, Lander F, Rietveld FJ. Transplantation of Descemet's membrane carrying viable endothelium through a small scleral incision. *Cornea.* 2002;21:415-418.
2. Terry MA, Ousley PJ. Deep lamellar endothelial keratoplasty in the first United States patients: early clinical results. *Cornea.* 2001;20:239-243.
3. Price FW Jr, Price MO. Descemet's stripping with endothelial keratoplasty in 50 eyes: a refractive neutral corneal transplant. *J Refract Surg.* 2005;21:339-345.
4. Mimura T, Yamagami S, Yokoo S, et al. Cultured human corneal endothelial cell transplantation with a collagen sheet in a rabbit model. *Invest Ophthalmol Vis Sci.* 2004;45:2992-2997.
5. Ishino Y, Sano Y, Nakamura T, et al. Amniotic membrane as a carrier for cultivated human corneal endothelial cell transplantation. *Invest Ophthalmol Vis Sci.* 2004;45:800-806.
6. Sumide T, Nishida K, Yamato M, et al. Functional human corneal endothelial cell sheets harvested from temperature-responsive culture surfaces. *FASEB J.* 2006;20:392-394.
7. Mimura T, Yamagami S, Yokoo S, et al. Sphere therapy for corneal endothelium deficiency in a rabbit model. *Invest Ophthalmol Vis Sci.* 2005;46:3128-3135.
8. Mimura T, Yokoo S, Araie M, Amano S, Yamagami S. Treatment of rabbit bullous keratopathy with precursors derived from cultured human corneal endothelium. *Invest Ophthalmol Vis Sci.* 2005;46:3637-3644.
9. Van Horn DL, Sendele DD, Seideman S, Buco PJ. Regenerative capacity of the corneal endothelium in rabbit and cat. *Invest Ophthalmol Vis Sci.* 1977;16:597-613.
10. Koizumi N, Sakamoto Y, Okumura N, et al. Cultivated corneal endothelial cell sheet transplantation in a primate model. *Invest Ophthalmol Vis Sci.* 2007;48:4519-4526.
11. Joyce NC, Harris DL, Mello DM. Mechanisms of mitotic inhibition in corneal endothelium: contact inhibition and TGF-beta2. *Invest Ophthalmol Vis Sci.* 2002;43:2152-2159.
12. Yoshida K, Kase S, Nakayama K, et al. Involvement of p27KIP1 in the proliferation of the developing corneal endothelium. *Invest Ophthalmol Vis Sci.* 2004;45:2163-2167.
13. Enomoto K, Mimura T, Harris DL, Joyce NC. Age differences in cyclin-dependent kinase inhibitor expression and rb hyperphosphorylation in human corneal endothelial cells. *Invest Ophthalmol Vis Sci.* 2006;47:4330-4340.
14. Mimura T, Joyce NC. Replication competence and senescence in central and peripheral human corneal endothelium. *Invest Ophthalmol Vis Sci.* 2006;47:1387-1396.
15. Zhu C, Joyce NC. Proliferative response of corneal endothelial cells from young and older donors. *Invest Ophthalmol Vis Sci.* 2004;45:1743-1751.
16. Engelmann K, Bohnke M, Friedl P. Isolation and long-term cultivation of human corneal endothelial cells. *Invest Ophthalmol Vis Sci.* 1988;29:1656-1662.
17. Miyata K, Drake J, Osakabe Y, et al. Effect of donor age on morphologic variation of cultured human corneal endothelial cells. *Cornea.* 2001;20:59-63.
18. Blake DA, Yu H, Young DL, Caldwell DR. Matrix stimulates the proliferation of human corneal endothelial cells in culture. *Invest Ophthalmol Vis Sci.* 1997;38:1119-1129.
19. Worthylake RA, Burridge K. RhoA and ROCK promote migration by limiting membrane protrusions. *J Biol Chem.* 2003;278:13578-13584.
20. Hall A. Rho GTPases and the actin cytoskeleton. *Science.* 1998;279:509-514.
21. Braga VM, Del Maschio A, Machesky L, Dejana E. Regulation of cadherin function by Rho and Rac: modulation by junction maturation and cellular context. *Mol Biol Cell.* 1999;10:9-22.
22. Kaibuchi K, Kuroda S, Amano M. Regulation of the cytoskeleton and cell adhesion by the Rho family GTPases in mammalian cells. *Annu Rev Biochem.* 1999;68:459-486.
23. Somlyo AP, Somlyo AV. Signal transduction by G-proteins, rho-kinase and protein phosphatase to smooth muscle and non-muscle myosin II. *J Physiol.* 2000;522;2:177-185.
24. Nakagawa O, Fujisawa K, Ishizaki T, Saito Y, Nakao K, Narumiya S. ROCK-I and ROCK-II, two isoforms of Rho-associated coiled-coil forming protein serine/threonine kinase in mice. *FEBS Lett.* 1996;392:189-193.
25. Olson MF, Ashworth A, Hall A. An essential role for Rho, Rac, and Cdc42 GTPases in cell cycle progression through G1. *Science.* 1995;269:1270-1272.
26. Croft DR, Olson MF. The Rho GTPase effector ROCK regulates cyclin A, cyclin D1, and p27Kip1 levels by distinct mechanisms. *Mol Cell Biol.* 2006;26:4612-4627.
27. Chen J, Guerriero E, Lathrop K, SundarRaj N. Rho/ROCK signaling in regulation of corneal epithelial cell cycle progression. *Invest Ophthalmol Vis Sci.* 2008;49:175-183.
28. Narumiya S, Ishizaki T, Uehata M. Use and properties of ROCK-specific inhibitor Y-27632. *Methods Enzymol.* 2000;325:273-284.
29. Insler MS, Lopez JG. Transplantation of cultured human neonatal corneal endothelium. *Curr Eye Res.* 1986;5:967-972.
30. Honjo M, Tanihara H, Kameda T, Kawaji T, Yoshimura N, Araie M. Potential role of Rho-associated protein kinase inhibitor Y-27632 in glaucoma filtration surgery. *Invest Ophthalmol Vis Sci.* 2007;48:5549-5557.
31. Roovers K, Assoian RK. Effects of rho kinase and actin stress fibers on sustained extracellular signal-regulated kinase activity and activation of G(1) phase cyclin-dependent kinases. *Mol Cell Biol.* 2003;23:4283-4294.
32. Swant JD, Rendon BE, Symons M, Mitchell RA. Rho GTPase-dependent signaling is required for macrophage migration inhibitory factor-mediated expression of cyclin D1. *J Biol Chem.* 2005;280:23066-23072.
33. Welsh CF, Roovers K, Villanueva J, Liu Y, Schwartz MA, Assoian RK. Timing of cyclin D1 expression within G1 phase is controlled by Rho. *Nat Cell Biol.* 2001;3:950-957.
34. Hu W, Bellone CJ, Baldassare JJ. RhoA stimulates p27(Kip) degradation through its regulation of cyclin E/CDK2 activity. *J Biol Chem.* 1999;274:3396-3401.
35. Kikuchi M, Zhu C, Senoo T, Obara Y, Joyce NC. p27kip1 siRNA induces proliferation in corneal endothelial cells from young but not older donors. *Invest Ophthalmol Vis Sci.* 2006;47:4803-4809.
36. Lee HT, Kay EP. Regulatory role of PI 3-kinase on expression of Cdk4 and p27, nuclear localization of Cdk4, and phosphorylation of p27 in corneal endothelial cells. *Invest Ophthalmol Vis Sci.* 2003;44:1521-1528.
37. Lee JG, Kay EP. Two populations of p27 use differential kinetics to phosphorylate Ser-10 and Thr-187 via phosphatidylinositol 3-kinase in response to fibroblast growth factor-2 stimulation. *J Biol Chem.* 2007;282:6444-6454.
38. Olson MF. Applications for ROCK kinase inhibition. *Curr Opin Cell Biol.* 2008;20:242-248.
39. Coleman ML, Marshall CJ, Olson MF. RAS and RHO GTPases in G1-phase cell-cycle regulation. *Nat Rev Mol Cell Biol.* 2004;5:355-366.
40. Croft DR, Sahai E, Mavria G, et al. Conditional ROCK activation in vivo induces tumor cell dissemination and angiogenesis. *Cancer Res.* 2004;64:8994-9001.
41. Shi J, Wei L. Rho kinase in the regulation of cell death and survival. *Arch Immunol Ther Exp (Warsz).* 2007;55:61-75.
42. Coleman ML, Olson MF. Rho GTPase signalling pathways in the morphological changes associated with apoptosis. *Cell Death Differ.* 2002;9:493-504.
43. Dubreuil CI, Winton MJ, McKerracher L. Rho activation patterns after spinal cord injury and the role of activated Rho in apoptosis in the central nervous system. *J Cell Biol.* 2003;162:233-243.

44. Watanabe K, Ueno M, Kamiya D, et al. A ROCK inhibitor permits survival of dissociated human embryonic stem cells. *Nat Biotechnol.* 2007;25:681-686.
45. Koyanagi M, Takahashi J, Arakawa Y, et al. Inhibition of the Rho/ROCK pathway reduces apoptosis during transplantation of embryonic stem cell-derived neural precursors. *J Neurosci Res.* 2008;86:270-280.
46. Moore M, Marroquin BA, Gugliotta W, Tse R, White SR. Rho kinase inhibition initiates apoptosis in human airway epithelial cells. *Am J Respir Cell Mol Biol.* 2004;30:379-387.
47. Svoboda KK, Moessner P, Field T, Acevedo J. ROCK inhibitor (Y27632) increases apoptosis and disrupts the actin cortical mat in embryonic avian corneal epithelium. *Dev Dyn.* 2004;229:579-590.
48. Kobayashi K, Takahashi M, Matsushita N, et al. Survival of developing motor neurons mediated by Rho GTPase signaling pathway through Rho-kinase. *J Neurosci.* 2004;24:3480-3488.
49. Hu E, Lee D. Rho kinase as potential therapeutic target for cardiovascular diseases: opportunities and challenges. *Expert Opin Ther Targets.* 2005;9:715-736.

ORIGINAL ARTICLE

Prospective Randomized Trial of Limbal Relaxing Incisions Combined With Microincision Cataract Surgery

Masayuki Ouchi, MD, PhD; Shigeru Kinoshita, MD, PhD

ABSTRACT

PURPOSE: To evaluate clinical outcomes of the limbal relaxing incision (LRI) combined with bimanual phacoemulsification and insertion of an intraocular lens (IOL) developed for bimanual microincision cataract surgery (MICS).

METHODS: In a prospective, single-center study, eyes with ≥0.75 diopters (D) of keratometric astigmatism were randomly assigned to two surgical techniques: 1) bimanual MICS (non-LRI group) or 2) LRI combined with bimanual MICS (LRI group). Postoperative uncorrected distance visual acuity (UDVA), corrected distance visual acuity (CDVA), postoperative refractive error, corneal topography, and vector analysis of keratometric change between pre- and postoperative eyes were compared.

RESULTS: In all cases of astigmatism in the LRI group, incisions for phacoemulsification and IOL insertion did not overlap or affect the LRIs. Uncorrected distance visual acuity was significantly higher in the LRI group (mean: 0.94), than in the non-LRI group (mean: 0.71, P=.009), although no difference was seen in CDVA in either group. Postoperative cylindrical error was significantly lower in the LRI group than in the non-LRI group (0.56 D and 1.51 D, respectively, P=.0004). Cravy analysis showed that the vector change in cylinder was 1.44 D in the LRI group and 0.18 D in the non-LRI group (P=.0007).

CONCLUSIONS: Limbal relaxing incision with bimanual MICS is an easy-to-follow combined surgery to correct preexisting astigmatism with predictable accuracy. [*J Refract Surg.* 2009;xx:xxx-xxx.] doi:10.3928/1081597X-

The limbal relaxing incision (LRI) is known to be a useful and convenient procedure for reducing astigmatism, especially after cataract surgery.[1,2] In this procedure, a pair of arc-shaped corneal incisions, 400 to 550 µm in depth, are made in the steep axis inside the surgical limbus, with the incision angle determined by the degree of astigmatism.[3] The LRI flattens the corneal sphere in the steep axis to decrease corneal refractive power. This procedure does not require an extensive amount of equipment capital investment and it can also be performed during cataract surgery to correct preexisting astigmatism,[2] thus resulting in an enhanced outcome for cataract surgery. However, conventional cataract removal and intraocular lens (IOL) implantation create astigmatism at various degrees and reduce the accuracy of astigmatism correction. Moreover, the phacoemulsification incision and LRI sometimes mutually interfere, depending on the astigmatism angle, because LRI involves one pair of 40° to 120° arc-shaped incisions at various angles, which can make combined surgery more technically difficult due to a reduction in corneal rigidity.

On the other hand, bimanual microincision cataract surgery (MICS) can be performed through a 0.9-mm incision using a 22-gauge phacoemulsification needle and a 22-gauge irrigating chopper,[4] and the newly developed Y-60H MICS IOL (Hoya Corp, Tokyo, Japan) can be inserted through a 1.6-mm incision.[5] We report the clinical results of LRI combined with a 0.9-mm incision bimanual phacoemulsification and implantation of the Hoya Y-60H MICS IOL.

PATIENTS AND METHODS

A prospective study was conducted in a single center between September 2007 and July 2008. Patients were ran-

From Ouchi Eye Clinic (Ouchi); and the Department of Ophthalmology, Kyoto Prefectural University of Medicine (Ouchi, Kinoshita), Kyoto, Japan.

The authors have no proprietary or financial interest in the materials presented herein.

Correspondence: Masayuki Ouchi, MD, PhD, Ouchi Eye Clinic, 47-1 Karahashi Rajomon-cho, Minami-ku, Kyoto 601-8453, Japan. Tel: 81 75 662 7117; Fax: 81 75 662 7118; E-mail: mouchi@skyblue.ocn.ne.jp

Received: February 6, 2009; Accepted: August 13, 2009

TABLE 1

Baseline Parameters for the Limbal Relaxing Incision (LRI) and Non-LRI Groups

Parameter	LRI Group	Non-LRI Group	*P* Value
Number of eyes	96	93	
Men:women	32:45	32:48	
Right eyes:left eyes	53:43	51:42	
Mean age±SD (range) (y)	70.8±7.9 (55 to 82)	63.7±8.2 (48 to 87)	
Mean spherical equivalent±SD (range) (D)	0.12±4.46 (−12.50 to 4.25)	0.68±3.10 (−5.25 to 3.50)	.33
Preoperative cylinder±SD (range) (D)	1.79±1.01 (0.75 to 3.00)	1.65±0.65 (0.75 to 3.00)	.68
UDVA±SD (range)	0.35±0.19	0.47±0.20	.54
CDVA±SD (range	0.51±0.48	0.58±0.56	.44

UDVA=uncorrected distance visual acuity (decimal converted from logMAR), CDVA= corrected distance visual acuity (decimal converted from logMAR)
LRI group denotes patients who underwent bimanual microincision cataract surgery with LRI.
Non-LRI group denotes patients who underwent bimanual microincision cataract surgery without LRI.
Note: Data for 3 of 192 patients were not included due to perioperative complications.

TABLE 2

Fukuyama's Nomogram for Limbal Relaxing Incision (LRI) to Correct Astigmatism With Phacoemulsification

	Arc to be Incised (°)	
Cylinder (D)	Against-the-Rule and Oblique Astigmatism	With-the-Rule Astigmatism
0.75	30	60
1.00	45	70
1.50	60	80
2.00	75	90
⩾3.00	90	110

Age (y)	LRI Incision Depth
Under 70	90% of central corneal thickness
70 to 80	85% of central corneal thickness
Over 80	80% of central corneal thickness

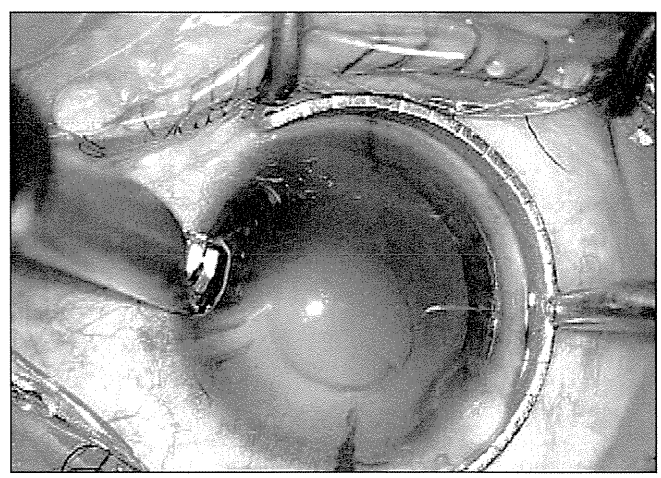

Figure 1. The limbal relaxing incision after lens extraction by 0.9-mm bimanual phacoemulsification.

domized by placing the patients' ID number in an envelope. The study population consisted of 192 eyes of 157 patients with ⩾0.75 diopters (D) of keratometric astigmatism in the healthy cornea and a corticonuclear cataract of grade 3 to 4. Patient age ranged from 48 to 87 years (mean: 67.2 years). All procedures were approved by the ethics committee of Ouchi Eye Clinic, and the study was conducted in accordance with the tenets of the Declaration of Helsinki. All operations were performed by the same surgeon (M.O.).

After obtaining informed consent, the patients were randomly assigned to two groups. Ninety-six eyes of 77 patients received LRI combined with bimanual MICS (LRI group) and 93 eyes of 80 patients received only bimanual MICS (non-LRI group). Baseline characteristics for the two groups are summarized in Table 1. Exclusion criteria included perioperative complications such as failure to place the IOL in the capsular bag, suturing of the wound, and any complication necessitating enlargement of the incision or insertion of another IOL. All patients were examined preoperatively and 6 months postoperatively. Zernike harmonic analysis of the topography data was used to measure the corneal regular astigmatism in the central 3-mm area obtained

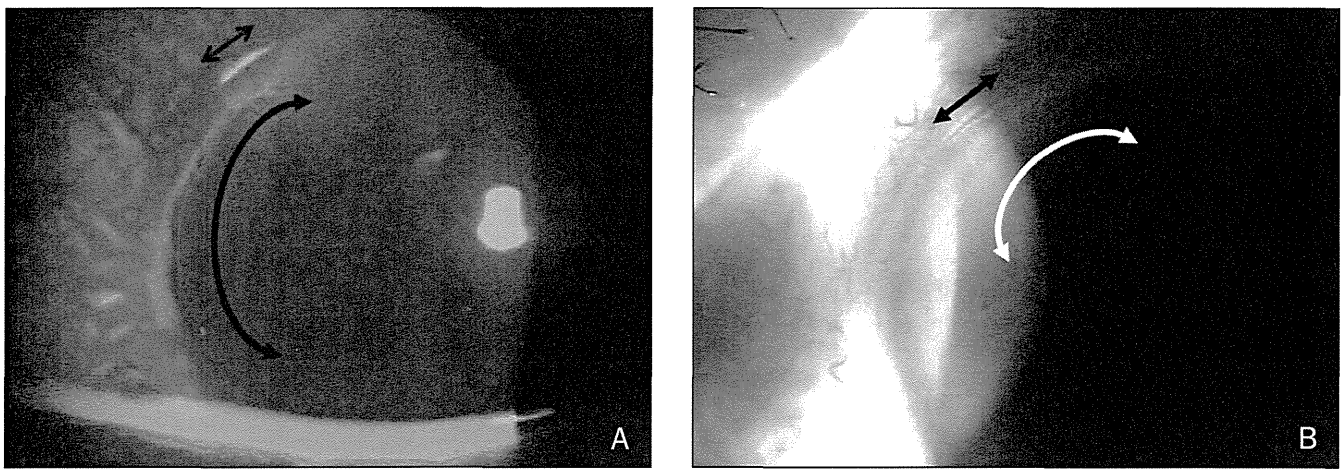

Figure 2. Postoperative examination of the 0.9-mm incision for phacoemulsification (arrowhead line) and limbal relaxing incision (arc line) do not mutually interact, even in the case of **A)** against-the-rule astigmatism or **B)** oblique astigmatism.

TABLE 3

Mean Postoperative Results for the Limbal Relaxing Incision (LRI) and Non-LRI Groups

	Mean±Standard Deviation (Range)		
Parameter	**LRI Group**	**Non-LRI Group**	***P* Value**
UDVA	0.94±0.34 (0.4 to 1.5)	0.71±0.52 (0.08 to 1.5)	.009
CDVA	1.12±0.30 (0.6 to 1.5)	1.18±0.31 (0.5 to 1.5)	.53
Spherical equivalent refraction in CDVA	0.50±0.35 (−1.5 to 1.5)	0.21±0.74 (−1.5 to 1.5)	.33
Cylindrical refraction in CDVA	0.56±0.87 (0 to 1.75)	1.51±0.79 (0.75 to 3.0)	.0004

UDVA=uncorrected distance visual acuity (decimal converted from logMAR), CDVA= corrected distance visual acuity (decimal converted from logMAR)
LRI group denotes patients who underwent LRI combined with bimanual microincision cataract surgery.
Non-LRI group denotes patients who underwent bimanual microincision cataract surgery without LRI.

with OPD-Scan II (NIDEK Co Ltd, Gamagori, Japan) and the Cravy vector analysis formula was used for evaluation of the results.[6] Postoperative uncorrected distance visual acuity (UDVA), corrected distance visual acuity (CDVA), and mean spherical equivalent and cylindrical refraction were also evaluated.

SURGICAL TECHNIQUE

Prior to surgery, three marks (two horizontal and one vertical) were made along the limbus using a 24-gauge needle with marker ink (Gentian Violet Marker Pad; BD [Becton, Dickinson and Co], Franklin Lakes, NJ) with the patient in a sitting position. Next, two 0.9-mm corneal incisions were made; one incision each at the 10- and 2-o'clock positions using a 0.9-mm MVR knife (EdgeAhead Stiletto, BD). A viscoelastic agent was injected via one of the incisions and continuous curvature capsulorrhexis was performed using a 26-gauge needle. Gentle hydrodissection and delineation was performed, followed by bimanual phacoemulsification using a 22-gauge phacoemulsification needle and an Agarwal 22-gauge irrigating chopper (MST, Redmond, Wash) through the 0.9-mm corneal incision. Bimanual cortex aspiration was then performed via the 0.9-mm corneal incision. After the capsule was filled with the viscoelastic agent, the steepest meridian was marked with a Fukuyama LRI 60° marker (ASICO, Westmont, Ill) at the peripheral cornea according to the corneal topography. The eyeball was fixed with a fixation ring, and the corneal limbus was incised using a diamond LRI knife (ASICO) at a preplanned angle depending on the degree of astigmatism and patient age-dictated Fukuyama's nomogram (Table 2, Fig 1). Preoperatively, central corneal thickness was measured using the AL-2000 biometer/pachymeter (Tomey Corp, Nagoya, Japan), and incision depth was determined based on central corneal thickness and patient age. If the patient was under 70 years old, the LRI incision depth was 90% of the central corneal thickness; 85% was used when patient age was between 70 and 80 years. If the patient was >80 years, the LRI incision depth was 80% of the central corneal thickness.

Even under strong pressure, the viscoelastic agent did not leak out though the 0.9-mm clear corneal incision and corneal distortion never occurred. The LRI in this surgical method can be performed as easily as LRI performed independently due to the excellent stability of the cornea, even after a lensectomy. In this tech-

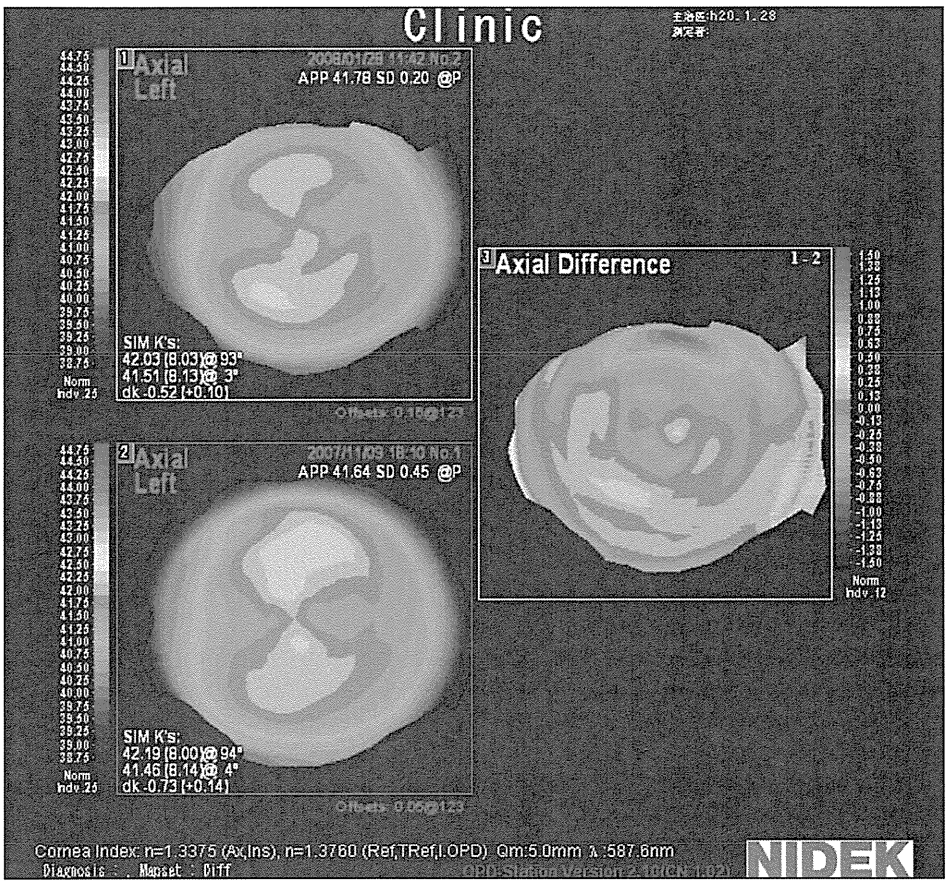

Figure 3. Corneal topography of a non-limbal relaxing incision case shows no change from **lower left)** preoperative to **upper left)** 3-month postoperative, and **right)** axial difference maps.

nique, a 0.9-mm phacoemulsification incision is made at the limbus and LRIs are made at 1 mm inside the limbus. After making one pair of LRIs, a new 1.6-mm clear corneal incision was made at an area of the cornea that was away from, and did not affect, the pair of arc-shaped LRIs. The IOL was inserted via the superior site in the case of against-the-rule astigmatism and in non-LRI cases, via the temporal site in the case of with-the-rule astigmatism, and via enlarged paracentesis in oblique astigmatism.

The Hoya Y-60H IOL was then inserted through the new 1.6-mm corneal incision.[5]

Statistical Analysis

Differences in all data were assessed using a 2-sided paired *t* test. A *P* value $<.05$ was considered statistically significant.

RESULTS

Of the 192 eyes initially enrolled in the study, 3 were excluded due to perioperative complications (2 due to failure to place the IOL in the bag and 1 due to posterior capsule rupture, necessitating the insertion of another IOL and wound suturing). No case of delayed or irregular healing associated with the LRI/cataract combined surgery was noted. In all cases of astigmatism, incisions for phacoemulsification and IOL insertion did not overlap or affect the LRIs (Fig 2). No significant difference between the two groups in preoperative UDVA (decimal converted from logMAR), CDVA (decimal converted from logMAR), and cylindrical refraction (Table 1) was noted. Table 3 shows mean postoperative UDVA, CDVA, spherical equivalent refraction, and cylindrical refraction. The LRI group registered significantly higher UDVA due to small postoperative corneal astigmatism, although no difference was seen in postoperative CDVA. The non-LRI group eyes showed small corneal topography changes between the pre- and postoperative periods; a typical case is shown in Figure 3. The Cravy vector analysis formula showed that the mean change of corneal regular astigmatism was 0.18 ± 0.13 D (range: 0.07 to 0.46) postoperatively. On the other hand, there was a marked corneal change in the LRI group eyes (Fig 4) and the mean change of corneal regular astigmatism was 1.44 ± 0.79 D (range: 0.20 to 3.45) (P=.0007). The pre- and postoperative corneal topography of a typical LRI-group eye is shown in Figure 4. A typical "bowtie pattern" was seen in preoperative topography but disappeared in postoperative topography.

DISCUSSION

Limbal relaxing incision/cataract combined surgery was first reported in 1998.[7] This procedure is now widely accepted by cataract surgeons due to its simplicity and relatively low investment required to purchase the associated surgical equipment compared with that needed for LASIK. Compared to astigmatic keratotomy,[8] LRI/cataract combined surgery has a low percentage of complications such as corneal perfora-

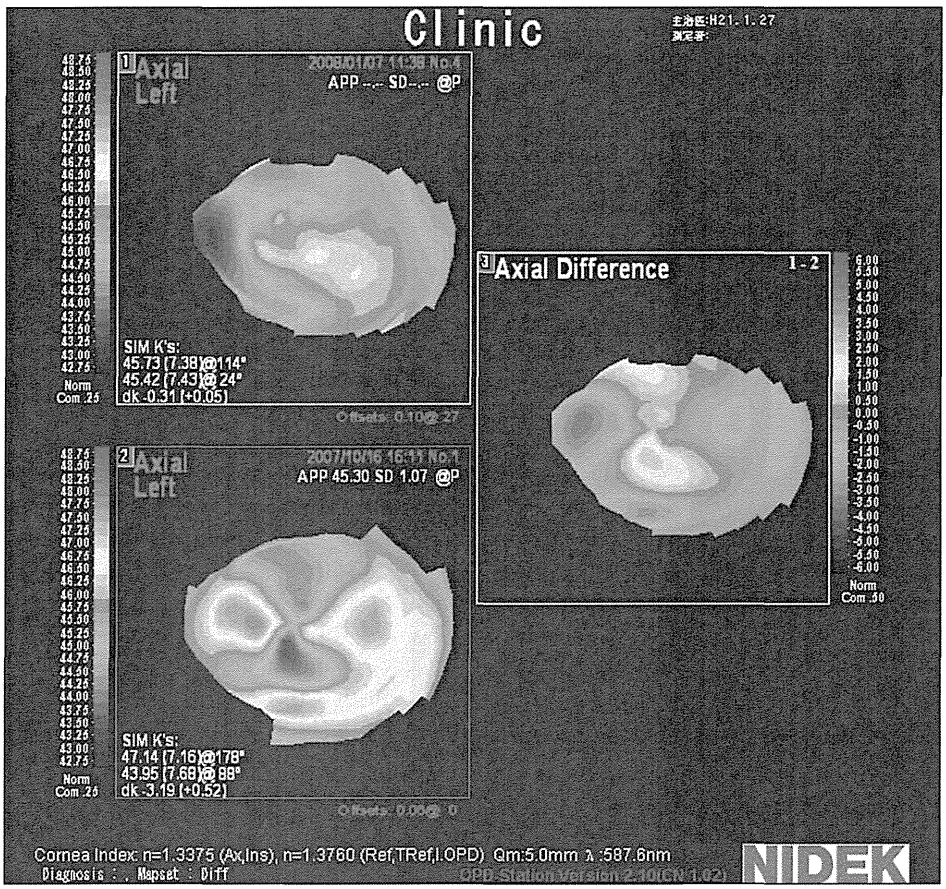

Figure 4. Corneal topography of a limbal relaxing incision case. **Lower left)** Preoperative topography map shows the typical bowtie pattern, but the **upper left)** 3-month postoperative map does not. **Right)** Axial difference map.

tion, axis shifts, or overcorrection. Moreover, the LRI does not affect intraocular visibility during cataract surgery as the incisions are made at the peripheral cornea. However, the effect of cataract surgery on postoperative astigmatism cannot be ignored entirely, even in conventional small-incision surgery, and it has been shown that the smaller surgical incision results in less postoperative astigmatism and corneal higher order aberrations.[9-11] Moreover, in the case of with-the-rule astigmatism, the superior incision used for cataract surgery sometimes affects the LRI, and in the case of against-the-rule astigmatism, the temporal corneal incision overlaps the LRI.

On the other hand, bimanual phacoemulsification using a 22-gauge instrument needs only a 0.9-mm corneal incision.[4] In addition, insertion of the IOL is accomplished via the 1.6-mm clear corneal incision,[5] an incision size small enough to enable surgeons to choose the most appropriate wound position independent of the phacoemulsification incision. With this technique, surgeons can insert the IOL far from the LRI in all cases and angles of astigmatism. This procedure thereby avoids affecting the corneal axis and construction of the LRI. Moreover, the topography and Cravy analysis performed in this study showed that the bimanual MICS with a 22-gauge instrument and MICS IOL insertion had little or no effect on keratometric change. This means that the combined LRI effect directly reflects the postoperative astigmatic change and can be performed with good predictable accuracy that is also due to the use of improved LRI nomograms such as the Nichamin nomogram.[3]

Limbal relaxing incision combined with 0.9-mm bimanual phacoemulsification and MICS IOL implantation is a useful procedure that can achieve accurate correction of preexisting astigmatism leading to good UDVA after cataract surgery.

AUTHOR CONTRIBUTIONS

Study concept and design (M.O., S.K.); data collection (M.O.); analysis and interpretation of data (M.O.); drafting of the manuscript (M.O.); critical revision of the manuscript (S.K.); statistical expertise (M.O.); administrative, technical, or material support (S.K.)

REFERENCES

1. Nichamin LD. Astigmatism control. *Ophthalmol Clin North Am.* 2006;19:485-493.
2. Müller-Jensen K, Fischer P, Siepe U. Limbal relaxing incisions

to correct astigmatism in clear corneal cataract surgery. *J Refract Surg.* 1999;15:586-589.

3. Nichamin LD. Nomogram for limbal relaxing incisions. *J Cataract Refract Surg.* 2006;32:1408.
4. Agarwal A, Agarwal A, Agarwal S, Narang P, Narang S. Phakonit: phacoemulsification through a 0.9 mm corneal incision. *J Cataract Refract Surg.* 2001;27:1548-1552.
5. Ouchi M. Using the HOYA Y-60H intraocular lens for micro-incision cataract surgery: early clinical results. *Japanese Journal of Cataract and Refractive Surgery.* 2008;22:67-72.
6. Cravy TV. Calculation of the change in corneal astigmatism following cataract extraction. *Ophthalmic Surg.* 1979;10:38-49.
7. Budak K, Friedman NJ, Koch DD. Limbal relaxing incisions with cataract surgery. *J Cataract Refract Surg.* 1998;24:503-508.
8. Oshika T, Shimazaki Y, Yoshitomi F, Oki K, Sakabe I, Matsuda S, Shiwa T, Fukuyama M, Hara Y. Arcuate keratotomy to treat corneal astigmatism after cataract surgery: a prospective evaluation of predictability and effectiveness. *Ophthalmology.* 1998;105:2012-2016.
9. Shepherd JR. Induced astigmatism in small incision cataract surgery. *J Cataract Refract Surg.* 1989;15:85-88.
10. Hayashi K, Yoshida M, Hayashi H. Postoperative corneal shape changes: microincision versus small-incision coaxial cataract surgery. *J Cataract Refract Surg.* 2009;35:233-239.
11. Yao K, Tang X, Ye P. Corneal astigmatism, high order aberrations, and optical quality after cataract surgery: microincision versus small incision. *J Refract Surg.* 2006;22:S1079-S1082.

AUTHOR QUERIES

Patients and Methods method of randomization was changed. Okay as edited?

Table 1, please provide range for UDVA and CDVA.

The mean and range of follow-up indicated in your reply to queries states 11.2 months (6 to 16 month), however, page 2 right column indicated follow-up was 6 months postoperative. Please clarify.

Table 3, please confirm range of Spherical Equivalent Refraction in CDVA as shown. Is it the same for both groups?

QUERIES PER DR WARING

Please indicate clearly in Methods, and in your nomogram table, that you are using a pair of incisions, and not just a single incision.

Is the 1998 Budak reference really the first description of limbal relaxing incisions with cataract surgery? As you know, transverse keratotomy is about 130 years old. I would be surprised if someone had not used transverse keratotomy with cataract surgery before 1998. Maybe you mean simultaneous surgery using limbal relaxing incisions only as opposed to other forms of transverse keratotomy not done simultaneously. Please clarify this in the Discussion text.

In your Discussion, please mention toric intraocular lenses as an alternative. I fully understand that you cannot include a detailed discussion of all methods of astigmatism correction, but I think you should at least briefly mention the role of toric IOLs as the most commonly used alternative to astigmatism correction with LRIs.